Quark Excitations Through the Prism of Direct Photon Plus Jet at the LHC

Satyaki Bhattacharya*, Sushil Singh Chauhan†, Brajesh Chandra Choudhary‡ and Debajyoti Choudhury§

Department of Physics and Astrophysics, University of Delhi, Delhi 110007, India.

The quest to know the structure of matter has resulted in various theoretical speculations wherein additional colored fermions are postulated. Arising either as Kaluza-Klein excitations of ordinary quarks, or as excited states in scenarios wherein the quarks themselves are composites, or even in theories with extended gauge symmetry, the presence of such fermions (q^*) can potentially be manifested in $\gamma + jet$ final states at the LHC. Using unitarized amplitudes and the CMS setup, we demonstrate that in the initial phase of LHC operation (with an integrated luminosity of $200\,\mathrm{pb}^{-1}$) one can discover such states for a mass upto 2.0 TeV. The discovery of a q^* with a mass as large as $\sim$5 TeV can be acheived for an integrated luminosity of $\sim 140\,\mathrm{fb}^{-1}$. We also comment on the feasibility of mass determination.

PACS numbers: 12.60.Rc, 13.40.-f, 13.85.Qk

I. INTRODUCTION

The replication of fermion families, while being of profound significance in our understanding of fundamental issues such as CP-violation and baryogenesis, nonetheless is puzzling in its own right. Despite its enormous success in explaining all observed phenomena in the regime of particle physics, the Standard Model (SM) has been entirely unable to proffer any insight into this aspect. Indeed, though the observed mass hierarchies and fermion mixings can easily be accommodated, the SM framework, by its very structure, is unable to even ask such questions of itself. This has led to various speculative ideas seeking to explain these ill-understood issues. Prominent among these are (*i*) models with extended (family) symmetry, (*ii*) constructions based on higher dimensional theory (with or without a string theory motivation) and (*iii*) the possibility of quark-lepton compositeness, namely that the SM fermions are not elementary at all.

Many of the ideas discussed in this article would be equally applicable—possibly with minor variations—to theories belonging to any of these three classes. However, for the sake of concreteness, we shall consider theories of compositeness as the basic template for our discussions. Part of the motivation lies in the fact of these theories having a more straightforward ultraviolet completion and, furthermore, suffering from a fewer number of extra channels, thereby reducing possible ambiguities.

In such theories, the fundamental constituents of matter, very often termed *preons*[1], are postulated to experience an hitherto unknown force on account of an asymptotically free but confining gauge interaction[2], which becomes very strong at a characteristic scale Λ, thereby leading to bound states (composites) to be identified with quarks and/or leptons. In many such models[3, 4], though not all, quarks and leptons share at least some common constituents.

Accepting this hypothesis would naturally lead to the existence of excited states of fermions at a mass scale comparable to the dynamics of the new binding force. In the simplest phenomenological models [5], the excited fermions are assumed to have both spin and isospin 1/2 and to have both their left- and right-handed components in weak isodoublets (*i.e.* they are vector-like). Similar is the case for, say higher-dimensional models wherein the known universe is constrained to be on a 4-dimensional subspace (a 3-brane) while the SM fields—in particular, the fermions—live in all the dimensions. The analogues of the excited fermions would be the Kaluza-Klein excitations with the mass scale being identified with the inverse of the compactification scale.

Given that the "excited states" do suffer the SM gauge interactions, these may be produced at high-energy colliders and, subsequently, would decay, radiatively, into an ordinary fermion and a gauge boson (photon, W, Z or gluon). At an e^+e^- collider, charged excited fermions could be pair-produced via s-channel (γ and Z) exchanges in collisions, while for excited neutrinos only Z exchange contributes. Although t-channel diagrams are also possible (W for ν_e^* and γ/Z for e^*), such contributions to the overall pair production cross-section are generally much smaller on account of the smallness of the cross-couplings [5] between the excited state, its SM counterpart and a gauge boson. This very same coupling, on the other hand, may be used to singly produce such states (through both s- and t-channel diagrams). The four LEP collaborations have used these (and other) modes to essentially rule out such excitations almost upto the kinematically allowed range [6]. At the HERA, on the other hand, both excited leptons and quarks may be produced singly through t-channel diagrams and these processes have been looked at without any positive results [7].

If quarks and leptons are composite particles made up of smaller constituents, phenomenological effects may be

*Email Address: bhattacharya.satyaki@gmail.com
†Email Address: sushil@fnal.gov
‡Email Address: brajesh@fnal.gov
§Email Address: debchou@physics.du.ac.in

observable at the LHC and might even show up at Tevatron once sufficiently large luminosities are accumulated and analysed. If the compositeness/excitation scale (Λ) is not too high, then excited quarks can be produced on shell, while at energies sufficiently below Λ such an eventuality would manifest itself as an effective four fermion contact interaction invariant under SM guage transformations [8, 9]. Based on phenomenological studies of flavour independent contact interactions for two photon production, the lower bound has been estimated to be $\Lambda_{\pm} > 2.88$ (3.24) TeV at 95% CL for an integrated luminosity of 100 (200) fb^{-1} [10] at the LHC.

Both the experiments at the Tevatron, the CDF and DØ, have searched for excited quarks. The latter are assumed to couple to the SM particles primarily through gauge couplings. Their most visible signature could be either pair production or single excited state production via quark-gluon fusion, provided the q^*qg coupling is sufficiently large. Enhanced dijet production rate with an invariant mass peak above the SM continuum is one of the prominent signals, extensively searched for at the Tevatron and the DØ collaboration has excluded the mass range of 200-720 GeV[11]. Similarly, the CDF collaboration has excluded a mass range of 80-570 GeV [12, 13] based on searches with various final states. In a similar vein, the CDF collaboration has put a lower bound of $\Lambda \geq 2.81$ GeV at 95% CL using the $q\bar{q} \rightarrow e\nu$ prcoess[14] whereas the DØ collaboration rules out $\Lambda \leq$ 2.0 TeV at 95% CL from diject mass peak searches[15].

At the LHC, both the ATLAS and the CMS collaborations have predicted the sensitivity in the dijet production mode. The ATLAS collaboration has xlaimed that the use nof dijet angular distributions would allow contact interactions to be probed upto Λ =10 TeV with a integrated luminosity of 700 pb^{-1}. The CMS collaboration, on the other hand, has estimated that $\Lambda = 6.2$ TeV can be excluded at 95% CL with a luminosity of 100 pb^{-1} and that 5σ sensitivity could be reached for Λ =8 TeV with just 1 fb^{-1} of data[16]. Recently, the possibility of top quark compositeness has been explored through the $pp \rightarrow t\bar{t}t\bar{t}$ production process and it has been estimated that a 5σ excess can be observed for a new state of 2 TeV [17].

As an effective tool for the measurement of gluon density inside the colliding hadrons and for precision test of pQCD predictions, the isolated γ+jet final state has been studied with great detail at the Tevatron collider[18, 19, 20] and fixed target experiments[21]. Since $\gamma + jet$ final state will be one of the key backgrounds for the $H \rightarrow \gamma\gamma$ search at the LHC, extensive isolation studies addressing all known issues have been performed with this process both theoretically and with detailed detector simulations. It is also an important background for many new physics scenario e.g. Large Extra Dimensions[22, 23], Randall Sundrum Gravitons[24] etc. It will, thus, be very interesting to look at γ+jet as a probe of excited quarks in view of the unprecedented energy scale at LHC and the in-depth knowledge of this process gleaned from previous experiments and studies.

The rest of the paper has been organized as follows. In section II we have discussed the effective Lagrangian for the theory and new physics contribution. In Sections III and IV, we respectively discuss the backgrounds and event generation. Section V describes the photon and jet algorithms used for the analysis. In section VI we discuss the smearings due to detector resolution effects. Section VII gives the details of kinematical variables used to separate the signal from the background whereas Section VIII deals with isolation study. The significance of signal and discovery are discussed in section IX and X respectively. In section XI we have presented the result of the analysis. Systematics is discussed in detail in section XII followed by our conclusions and outlook.

II. NEW PHYSICS CONTRIBUTION TO $\gamma + Jet$ PRODUCTION

With our interest lying not in the pair-production of such excited states, but rather on their contribution to the photon plus single jet rates at a hadronic collider, we confine ourselves to examining only the relevant part of the Lagrangian, namely the (chromo-)magnetic transition between ordinary and excited states. In general, these may be parametrized by

$$\mathcal{L}_{int} = \frac{1}{2\,\Lambda} \bar{q^*_R}\, \sigma^{\mu\nu} \left[\sum_i g_i\, b_i\, T^a_i\, G^a_{i\,\mu\nu} \right] q_L + h.c., \quad (1)$$

where the index i runs over the three SM gauge groups, viz. $SU(3)$, $SU(2)$ and $U(1)$ and g_i, $G^a_{i\,\mu\nu}$ and T^a_i are the corresponding gauge couplings, field strength tensors and generators respectively. The dimensionless constants b_i are, *a priori*, unknown and presumably of order unity. With these determining both the production rates and the branching into various modes, clearly, the phenomenology would depend considerably on their (relative) sizes. In this article, we shall make the simplifying assumption that the excited states do not couple at all to the weak gauge bosons, but do so with the gluons and the photon. At first glance, this might seem incompatible with a $SU(2) \otimes U(1)$ invariant structure. However, complicated embeddings could be the answer. More than this, since the assumption would not change the results qualitatively, it, at least, has the merit of reducing the number of possible couplings and hence simplifying the analysis.

A further point needs to be noted here. With the Lagrangian of eq.(1) being a higher dimensional operator, the cross sections would typically grow with the center of mass energy, consequently violating unitarity. This is not unexpected in an effective theory as the term in eq.(1) is only the first term and the loss of unitarity, to a given order, is presumably cured once suitable higher dimensional operators are included. An equivalent way to achieve the same goal is to consider the b_i to be form

factors rather than constants. To this end, we shall define the $q^*q\gamma$ and q^*qg vertices to be given by

$$\begin{aligned} \overline{q^*}\, q\, \gamma_\mu(p): &\quad \frac{e\, e_q\, f_1}{\Lambda}\left(1+\frac{Q^2}{\Lambda^2}\right)^{-n_1}\ \sigma_{\mu\nu}\, p^\nu \\ \overline{q^*}\, q\, g_\mu(p): &\quad \frac{g_s f_3}{\Lambda}\left(1+\frac{Q^2}{\Lambda^2}\right)^{-n_3}\ \sigma_{\mu\nu}\, p^\nu\, T_\alpha \end{aligned} \tag{2}$$

where Q denotes the relevant momentum transfer and $f_i \sim 1$ are dimensionless constants related to b_i of eqn.(1). It can be checked that, for $Q^2 = s$, unitarity is restored as long as the constants $n_i \geq 1$. From now on, eqn.(2) defines our theory[1]. For the rest of our analysis, we shall confine ourselves to a discussion of $n_i = 1$. While this might seem to be an optimistic choice, it is not quite so. In fact, the collider search limits in the literature actually correspond to $n_i = 0$ and, thus, our limits would be more conservative.

With the aforementioned Lagrangian, the width of the $q*$ is given by

$$\begin{aligned} \Gamma(q*) &= \Gamma_{q+g} + \Gamma_{q+\gamma} \\ \Gamma_{q+g} &= \frac{2\alpha_s f_3^2}{3}\,\Gamma_0 \\ \Gamma_{q+\gamma} &= \frac{e_q^2 \alpha f_1^2}{2}\,\Gamma_0 \\ \Gamma_0 &\equiv \frac{M_{q^*}^3}{\Lambda^2}\left(1-\frac{4m_q^2}{M_{q^*}^2}\right)\left(1-\frac{m_q^2}{M_{q^*}^2}\right)^2 \end{aligned} \tag{3}$$

and can be very large for a heavy q^* (see Table I). As a fat resonance is often difficult to observe, this will turn out to have profound consequences.

TABLE I: $\Gamma(q*)$ as a function of $M_{q*}(=\Lambda)$ for different coupling strengths. Both α_s and α_{em} are evaluated at M_{q^*}.

M_{q*}	Γ (GeV)	
(TeV)	$f_1 = f_3 = 1.0$	$f_1 = f_3 = 0.5$
0.5	34.4	8.61
1.0	63.6	15.9
2.0	118	29.6
3.0	170	42.6
4.0	221	55.2
5.0	271	67.6
6.0	319	79.8
7.0	367	91.8

With the introduction of these (flavour-diagonal) vertex as in eq.(2), the subprocess $qg \to q\gamma$ acquires a new

[1] While a Lagrangian formulation leading to such vertices would necessitate a seemingly non-local Lagrangian, this is not unexpected in an effective theory.

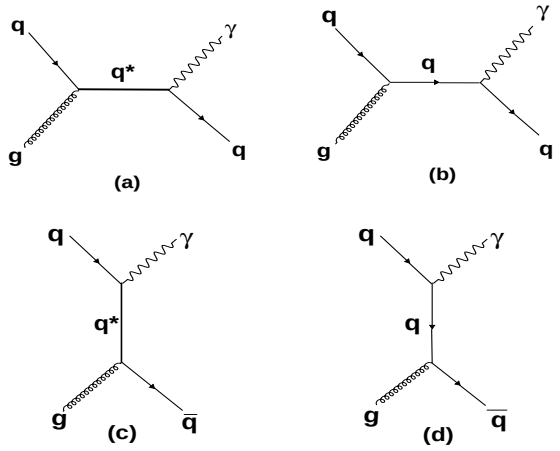

FIG. 1: Production of $\gamma + Jet$ final state through excited quark mediation (a & c) as well as SM processes (b & d).

contribution as portrayed in Fig.1(a). Adding this contribution to the pure QCD one, the ensuing differential cross section reads

$$\begin{aligned} \left.\frac{d\sigma}{d\hat{t}}\right|_{qg\to q\gamma} &= \frac{-\pi\,\alpha\,\alpha_s\,e_q^2}{3\,\hat{s}^2}\left[C_{sm} + 2\frac{f_1 f_3}{\Lambda^2}C_I + \frac{f_1^2 f_3^2}{\Lambda^4}C_Q\right] \\ C_{sm} &\equiv \frac{\hat{u}}{\hat{s}} + \frac{\hat{s}}{\hat{u}} \\ C_I &\equiv \frac{\hat{s}^2\,(\hat{s}-M_{q^*}^2)\,\mathcal{F}_s}{(\hat{s}-M_{q^*}^2)^2+\Gamma^2 M_{q^*}^2} + \frac{\hat{u}^2\,\mathcal{F}_u}{\hat{u}-M_{q*}^2} \\ C_Q &\equiv \left(\hat{s}\hat{u}+M_{q^*}^2 t\right) \left[\frac{\hat{s}^2\,\mathcal{F}_s^2}{(\hat{s}-M_{q^*}^2)^2+\Gamma^2 M_{q^*}^2} + \frac{\hat{u}^2\,\mathcal{F}_u^2}{(\hat{u}-M_{q^*}^2)^2}\right] \\ &\quad + 2M_{q^*}^2\,\frac{\hat{s}\hat{t}\hat{u}}{\hat{u}-M_{q^*}^2}\,\frac{(\hat{s}-M_{q^*}^2)\,\mathcal{F}_s\,\mathcal{F}_u}{(\hat{s}-M_{q^*}^2)^2+\Gamma^2 M_{q^*}^2} \\ \mathcal{F}_s &\equiv \left(1+\hat{s}/\Lambda^2\right)^{-(n_1+n_3)} \\ \mathcal{F}_t &\equiv \left(1-\hat{t}/\Lambda^2\right)^{-(n_1+n_3)} \\ \mathcal{F}_u &\equiv \left(1-\hat{u}/\Lambda^2\right)^{-(n_1+n_3)} \end{aligned} \tag{4}$$

with the SM result being recovered in the limit $\Lambda \to \infty$. The new physics contribution to the differential cross section thus depends on four parameters, namely f_1, f_3, Λ and the mass of the excited state M_{q^*}. For simplicity, we assume these to be flavour-independent (within a generation, it obviously has to be so). For eq.(1) to make sense as an effective Lagrangian, the masses have to be less than Λ (Ref.[25] requires that $M_{q^*} < \Lambda/\sqrt{2}$). Note that as long as $\Lambda \gg \hat{s}$, one of $f_{1,3}$ can always be absorbed in Λ. In our analyses, we would be considering only moderate values for these parameters.

For $q\bar{q} \to g\gamma$, the Feynman diagrams are as in Fig.1(c-d); the differential cross-sections are related to those in

eqn.(4) by crossing symmetry and are given by

$$\begin{aligned}
\left.\frac{d\sigma}{d\hat{t}}\right|_{q\bar{q}\to g\gamma} &= \frac{8\pi\,\alpha\,\alpha_s\,e_q^2}{9\,\hat{s}^2}\left[B_{sm} - 2\frac{f_1 f_3}{\Lambda^2}B_I + \frac{f_1^2 f_3^2}{\Lambda^4}B_Q\right] \\
B_{sm} &\equiv \frac{\hat{u}}{\hat{t}} + \frac{\hat{t}}{\hat{u}} \\
B_I &\equiv \frac{\hat{t}^2\,\mathcal{F}_t}{\hat{t} - M_{q^*}^2} + \frac{\hat{u}^2\,\mathcal{F}_u}{\hat{u} - M_{q^*}^2} \\
B_Q &\equiv \hat{t}\hat{u}\left[\frac{\hat{t}^2\,\mathcal{F}_t^2}{(\hat{t} - M_{q^*}^2)^2} + \frac{\hat{u}^2\mathcal{F}_u^2}{(\hat{u} - M_{q^*}^2)^2}\right] \\
&+ M_{q^*}^2\,\hat{s}\left[\frac{\hat{t}\,\mathcal{F}_t}{\hat{t} - M_{q^*}^2} + \frac{\hat{u}\,\mathcal{F}_u}{\hat{u} - M_{q^*}^2}\right]^2
\end{aligned} \tag{5}$$

III. BACKGROUNDS

The γ+jet final state can be mimicked by many known processes of the SM. We consider all the leading contributions (both the physics backgrounds as well as the detector ones) and broadly categorize these into three classes viz.,

- Type-I: where a photon and a hard jet is produced in the hard scattering.
- Type-II: QCD dijet, where one of the jets fragments into a high E_T π^0 which then decays into a pair of overlapping photons and, hence, is registered as a single photon. Moreover, in some cases the electromagnetic fraction of a jet can mimic a photon in the detector.
- Type-III: Photon + dijet production, where one of the jets is either lost or mismeasured. This could proceed either from hard processes such as $q\bar{q} \to q\bar{q}\gamma, gg\gamma$ (with all possible interchanges of initial and final state partons) or result from $W/Z + \gamma$ production with the heavy bosons decaying into a pair of jets.

While the leading contributions to the Type-I background emanates from the SM amplitudes of Fig. 1, a further contribution is displayed in Fig.2. In Figs.3 & 4, we show the major contributing Feynman diagrams for the Types II & III backgrounds respectively.

At the LHC, the Type-I background is dominated by the Compton process ($qg \to \gamma q$), while the other two subprocesses, namely anihilation($q\bar{q} \to \gamma g$) and gluon fusion ($gg \to \gamma g$) contribute only a small fraction in the low transverse momentum (P_T) ranges. For higher P_T, the annihilation subprocess can contribute upto about $\sim 23\%$ of the total Type-I background.

The Type-II background accrues mainly from $qg \to qg$, $q\bar{q} \to q\bar{q}$ and $gg \to gg$. For $\hat{P}_T \geq 200$ GeV (here $\hat{P}_T$ is the P_T of the outgoing partons in center of momentum frame

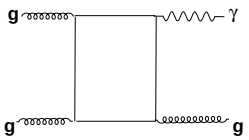

FIG. 2: Type-I Background: Additional contribution from gluon fusion. Lowest order background emanates from (b) and (d) in Fig.1.

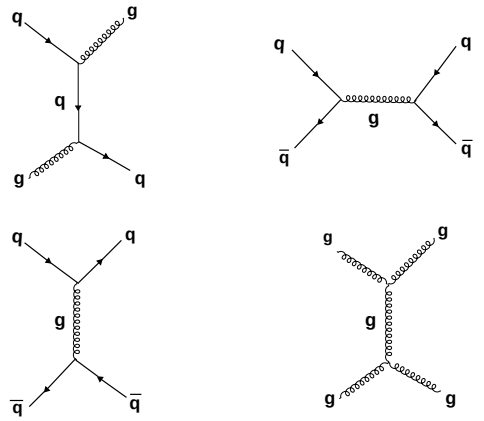

FIG. 3: Type-II Background: QCD jet production where a jet fakes a photon giving a $\gamma + Jet$ final state.

in a $2 \to 2$ hard scattering process), the total production cross section is $\sim 10^4$ times larger than the Type-I background. However, the fact of the probability of a jet faking a photon in the detector being $\sim 10^{-3} - 10^{-4}$ reduces the Type-II background to the same order as the Type-I. Moreover, for high transverse momenta the QCD dijet falls very rapidly ($\sim P_T^{-4}$), thereby suggesting a simple mechanism of suppressing this background

Although the total Type-III background is very small compared to the others, for the P_T range under consideration in this analysis, it turns out to be of the same order as $gg \to \gamma g$. And while nonresonant subprocesses (such as the $\mathcal{O}(\alpha_s^2\alpha)$ contributions to $q\bar{q} \to q\bar{q}\gamma$ or $gg \to q\bar{q}\gamma$) can, in principle, be substantial, note that these, in some sense are related to the much larger Type-I and Type-II backgrounds. Consequently, the former are typically suppressed when appropriate phase space cuts are imposed

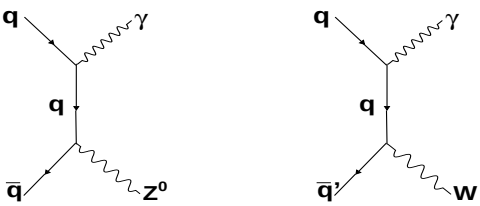

FIG. 4: Type-III Background: Here W/Z^0 decays to two jets and only one of the jets passes the trigger threshold.

TABLE II: Production cross section in different $\hat{P}_T$ bins for various Standard Model backgrounds with $\gamma + Jet$ final state.

Subprocess	50-100 GeV (pb)	100-200 GeV (pb)	200-400 GeV (pb)	400-600 GeV (pb)	600-1000 GeV (pb)	1000-1500 GeV (pb)	1500 GeV and above (pb)
$qg \to \gamma q$	7.22×10^3	569	36.3	1.53	2.22×10^{-1}	1.19×10^{-2}	7.6×10^{-4}
$q\bar{q} \to \gamma g$	652	65.3	5.56	3.18×10^{-1}	5.67×10^{-2}	3.76×10^{-3}	2.8×10^{-4}
$gg \to \gamma g$	1.79	8.6×10^{-2}	3.1×10^{-3}	7.04×10^{-5}	6.32×10^{-6}	1.75×10^{-7}	5.8×10^{-9}
QCD Jet	1.71×10^7	9.70×10^5	4.44×10^4	1.39×10^3	171	8.19	5.34×10^{-1}
[a]$Z(jj) + \gamma$	5.08	8.49×10^{-1}	9.50×10^{-2}	6.23×10^{-3}	1.16×10^{-3}	8.48×10^{-5}	6.46×10^{-6}
[a]$W(jj) + \gamma$	4.80	6.93×10^{-1}	6.19×10^{-2}	4.16×10^{-3}	7.39×10^{-4}	4.67×10^{-5}	2.99×10^{-6}

[a]Here the branching fraction is taken into account.

to reduce the latter.

In Table-II we show the production cross section for all backgrounds in different $\hat{P}_T$ ranges.

IV. EVENT GENERATION & CUTS

The event generation for signal and different background processes was done with PYTHIA-v6.325 [26]. For signal event generation the matrix elements of Eq. (4) and (5) were implemented inside the PYTHIA framwork. We used the following common parameters and PYTHIA switches:

- Parton Distribution Function(PDFs): CTEQ 5L [27];
- $Q^2 = \hat{s}$;
- MultiParton Interaction(MPI): "ON";
- Initial State Radiation(ISR) and Final State Radiation (FSR): "ON".

To get enough statistics for both the signal and the backgrounds, we divided the whole analysis into three phase space regions determined by the value of the P_T of the final state γ and the jet. For this purpose, the following $\hat{P}_T$ (CKIN(3) parameter of PYTHIA) criteria were used for different mass points of signal:

- $\hat{P}_T \geq 180$ GeV: 1.0–3.0 TeV,
- $\hat{P}_T \geq 450$ GeV: 3.5–4.5 TeV,
- $\hat{P}_T \geq 950$ GeV: 5.0–6.0 TeV.

A total of 16 mass points, 11 for coupling strength $f_1 = f_3 = 1.0$ (with a step size of 0.5 TeV) and 5 for $f_1 = f_3 = 0.5$ were generated. The different backgrounds were also generated in various $\hat{P}_T$ range. No pseudorapidity restriction was applied while generating the events as the large $\hat{P}_T$ cut requirement naturally restricts the events to well within $|\eta| < 5.0$. We must also mention here that in the final selection of γ, we have used the fiducial volume of the electromagnetic calorimeter of the CMS detector i.e. $|\eta| \leq 2.5$ with $1.444 \leq |\eta| \leq 1.566$ excluded on account of the insensitive region between the barrel and the endcaps[28]. The jets were selected up to $|\eta| \leq 3.0$ only, because of poor resolution in the forward calorimeter.

Fig. 5 shows the deviation in the total cross-section of $qg \to \gamma + jet$ as function of $M_{q^*}(= \Lambda)$. Clearly, the variation is well-approximated by a Λ^{-2} contribution superimposed upon a constant (the SM value). This is reflective of the fact that, for large Λ, the new physics contribution is dominated by the interference term in Eqs.(4,5) rather than the pure Λ^{-4} term . Only if we had imposed harder cuts on the photons, would the latter term have dominated (albeit at the cost of reducing event numbers and hence the sensitivity).

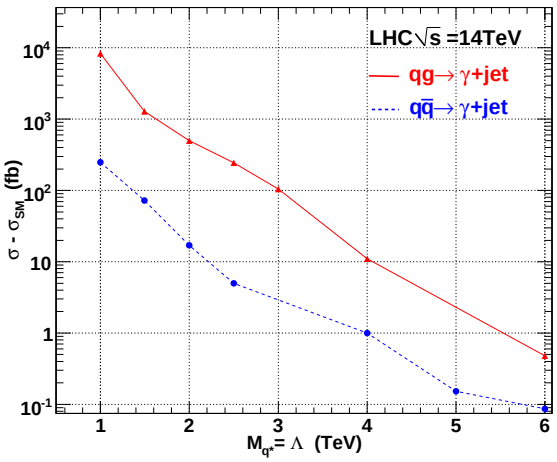

FIG. 5: Deviation of cross section from SM with $M_{q^*}(= \Lambda)$ at $\sqrt{s} = 14$ TeV.

V. PHOTON AND JET CANDIDATES AT THE GENERATOR LEVEL

Although a mass peak in the signal will appear as an excess of events over the continuum SM background, the significance for such an observation will depend on the size of this continnum. Hence, to enhance the signal peak, it is neccessary to reduce the background as much as possible. For the signal under investigation, QCD di-jet is the largest background, as it mimics γ+jet final state when one of the jet fakes a photon. To estimate this background reasonably at the generator level, it is a must to have a proper understanding of the reconstruction algorithm for a specific design of the detector rather than limit ourselves to only partonic level photon and jets from the final state in an event.

Taking this into consideration, we have used a clustering algorithm to account for fake photons arising from jets [29]. The electromganetic calorimeter (ECAL) of the CMS detector is made up of $PbWO_4$ crystals and each crystal covers 0.0175×0.0175 (equivalently, 1°) in the $\Delta\eta - \Delta\phi$ space (ϕ being the azimuthal angle). For photon reconstruction, we have used the "hybrid" algorithm[30] where we consider only those final state electromagnetic particles (i.e., γ, e^+ and e^-) in the $\eta - \phi$ space such that neither of the distances $\Delta\eta$ and $\Delta\phi$ from the seed object exceeds 0.09. This extension is equivalent to a 10×10 crystal size in the CMS detector. The seed for such a clustering must have a minimum P_T of 1 GeV. A photon candidate is either a direct photon or other electromagnetic obejcts such as $\pi^0 \to \gamma\gamma, \rho^0 \to \gamma\gamma$ etc. The main contribution of fake photons comes from $\pi^0 \to \gamma\gamma (\sim 81\%)$, $\eta \to \gamma\gamma (\sim 12\%)$ while other sources give only a small contribution. A detailed discussion of this reconstruction algorithm at the generator level can be found in a previous work [31].

For jet reconstruction, various algorithms have been used by different collider experiments. These include the MidpointCone [32], IterativeCone [33, 34], and the K_t algorithms [35, 36, 37]. The K_t and MidPoint algorithms are used mostly for offline analysis. Since we have used the CMS setup in our analysis, we use the IterativeCone algorithm to reconstruct jets at the generator level. Being much faster, this is commonly used for software based triggers. While the first algorithms for the jets at the hadron colliders started with simple cones in the $\Delta\eta - \Delta\phi$ space [38], clustering techniques have greatly improved in sophistication over the last two decades [32, 35].

For a real detector, the first step in the reconstruction, before invoking the jet algorithm, is to apply noise and pile-up suppression with a set of cuts on E_T. To make "perfect detector jets", we used a seed P_T cut on the P_T-ordered final state particles and selected only those which had a transverse momentum above the required minimum[2] of $P_{T seed} \geq 1.0$ GeV. Once the seed is selected, we search around for all the particles in a cone of $\Delta R \leq 0.5$. The objects inside the cone are used to calculate a *proto-jet* direction and energy using the E-scheme($\sum P_i$). The computed direction is then used to seed a new proto-jet. The procedure is repeated until both the energy and the direction of the putative jet is stable between iterations. We quantify this by requiring that the energy should change by less than 1% and the direction by less than $\Delta R = 0.01$. When a stable proto-jet is found, all objects in the proto-jet are removed from the list of input objects and the stable proto-jet is added to the list of jets. The whole procedure is repeated until the list is bereft of objects with an E_T above the seed threshold. The cone size and the seed threshold are the parameters of the algorithm.

VI. SMEARING EFFECTS

While a detailed and full-scale detector simulation is beyond the scope of this work, realistic detector effects can easily be approximated. To this end, we smear the generator level information with ECAL and HCAL resolutions of the CMS detector.

For the ECAL resolution function, we use the form

$$\frac{\delta E}{E} = \frac{a}{\sqrt{E}} \oplus \frac{a_n}{E} \oplus C \tag{6}$$

where a denotes the stochastic term, a_n is the white noise term and C is the constant term, with the three contributions being added in quadrature. For each of these terms, we use values identical to those for the electromagnetic calorimeter of the CMS [30], namely

$$\begin{aligned} C &= 0.55\% \\ a_n &= \begin{cases} 2.1 \times 10^{-3}\,\text{GeV} & |\eta| < 1.5 \\ 2.45 \times 10^{-3}\,\text{GeV} & 1.5 \leq |\eta| \leq 2.5 \end{cases} \\ a &= \begin{cases} 2.7 \times 10^{-2}\,\text{GeV}^{1/2} & |\eta| < 1.5 \\ 5.7 \times 10^{-2}\,\text{GeV}^{1/2} & 1.5 \leq |\eta| \leq 2.5\ . \end{cases} \end{aligned}$$

The resolutions for $\Delta\eta$ and $\Delta\phi$ were taken to be 0.02 and 0.001 respectively for both the barrel and endcap.

For the hadronic calorimeter, the resolutions were once again assumed to be the same as those for the CMS HCAL [39, 40], namely,

- Barrel:

$$\frac{\delta E}{E} = \frac{65\%}{\sqrt{E/\,\text{GeV}}} \oplus 5\%, \Delta\eta = 0.04, \Delta\phi = 0.02$$

- Endcaps:

$$\frac{\delta E}{E} = \frac{83\%}{\sqrt{E/\,\text{GeV}}} \oplus 5\%, \Delta\eta = 0.03, \Delta\phi = 0.02$$

[2] The seed threshold can vary from 0.5 to 2.0 GeV depending on the energy of reconstructed jet.

- Forward region:

$$\frac{\delta E}{E} = \frac{100\%}{\sqrt{E/\,\mathrm{GeV}}} \oplus 5\%, \Delta\eta = 0.04, \Delta\phi = 0.04\ .$$

The four momenta of the photon and jet were recalculated after applying these resolution effects using an appropriate Gaussian smeared function. In Fig. 6, we show the effect of resolution on the mass peak for a M_{q^*} of 1 TeV.

It should be noted that the ATLAS detector at the LHC has a better jet energy resolution with the constant term being ∼2 % [41] compare to ∼5 % in the CMS detector. On the other hand, the CMS ECAL has a better resolution than the ATLAS one owing to a smaller constant term. However, with the resolving power being dominated by the jet energy resolution, ATLAS should do somewhat better. In other words, our results correspond to a *conservative* choice.

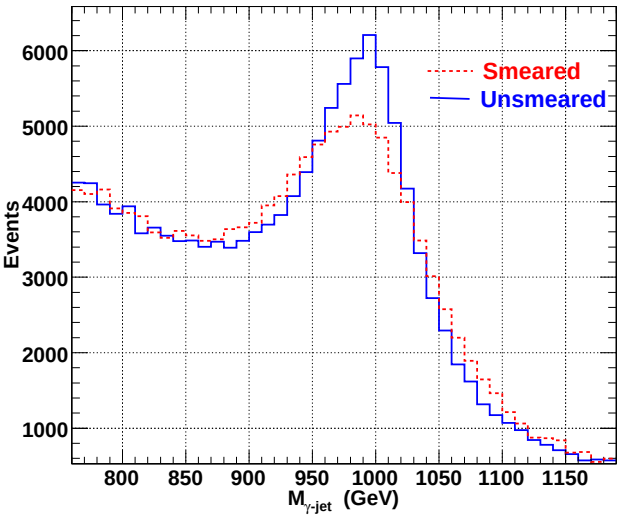

FIG. 6: Effect of smearing on the mass peak for an excited quark of 1 TeV.

VII. KINEMATICAL VARIABLES

In Fig. 7, we show the kinematical distributions for the leading photon and the leading jet for $P_T^{\gamma,jet} \geq 200$ GeV dataset for the background and the signal for M_{q^*} =1 TeV. For purpose of visual clarity, the distributions for $Z+\gamma$ and $W+\gamma$ backgrounds have been scaled up by a factor of 10. The bump in the transverse momentum distributions are primarily driven by the on-shell production of the q^* and, therefore, are centred slightly below $M_{q^*}/2$. As is evident from Fig. 7(e), an excess in the invariant mass spectrum would be quite prominent for even $\int L.dt$ =1pb^{-1}. The t-channel contribution has been included and manifests itself in the elongation of the side

TABLE III: Preselection-efficiency and geometrical acceptence for various SM backgrounds and few signal points.

Selection Cut	Signal %	$\gamma + Jet$ %	QCD %	$Z+\gamma$ %	$W+\gamma$ %
$P_T^{\gamma,jet} \geq 200GeV$	48.7 [1 TeV]	44.2	0.90	38.4	37.1
$P_T^{\gamma,jet} \geq 500GeV$	40.2 [4 TeV]	39.8	0.42	50.4	50.6
$P_T^{\gamma,jet} \geq 1TeV$	47.4 [5 TeV]	46.0	0.51	58.8	59.9
$\lvert\eta^\gamma\rvert \leq 2.5$, $\lvert\eta^{jet}\rvert \leq 3.0$, $\lvert\eta^\gamma\rvert \notin [1.4442, 1.5666]$	42.4 [1 TeV]	38.2	0.81	32.8	33.2
	38.2 [4 TeV]	37.8	0.40	47.4	48.4
	46.4 [5 TeV]	45.0	0.50	56.3	58.7

bands. It may be noted that the QCD dijet background is more than 10 times as large as the signal, but falls very rapidly with $P_T^{\gamma/\mathrm{jet}}$ (the mistagging probability has already been included). Fig. 7(f) shows the distribution in the subprocess center of mass scattering angle, with $\cos\theta^* = \tanh[(\eta^\gamma - \eta^{jet})/2.0]$. Note that major differences between the signal and background profile occur only for p_T and invariant mass distributions, whereas the other phase space variables are not very sensitive discriminants.

Fig. 8 shows similar distributions as in Fig. 7 but for the $M_{q^*} = 5$ TeV point instead. For these distributions we have used a $P_T^{\gamma,jet}$ cut of 1 TeV at the pre-selection level. With the P_T spectrum for the photon from QCD background falling very rapidly, the signal dominates over the background above 2 TeV even without isolation cuts. As for the corresponding invariant mass ($M_{\gamma-jet}$) distribution—see Fig. 8(e)— a combination of the large natural width and smearing effects results in a broad bump rather than a sharp one. Once again, the other distributions do not discriminate between the signal and background in any forceful manner. While the the slight dip in the central η^γ region for the $W+\gamma$ process might seem intriguing (especially in the absence of any such dip in the $Z+\gamma$ distribution), it is but a straightforward reflection of the well-known Radiation-Amplitude-Zero (RAZ) present in the former [42, 43]. That the RAZ in the angular distributuion is apparent only for the high $P_T^{\gamma,jet}$ cutoff case can be understood by realising that the rapidity of the photon as measured in the laboratory can be related to the rapidity (scattering angle) in the

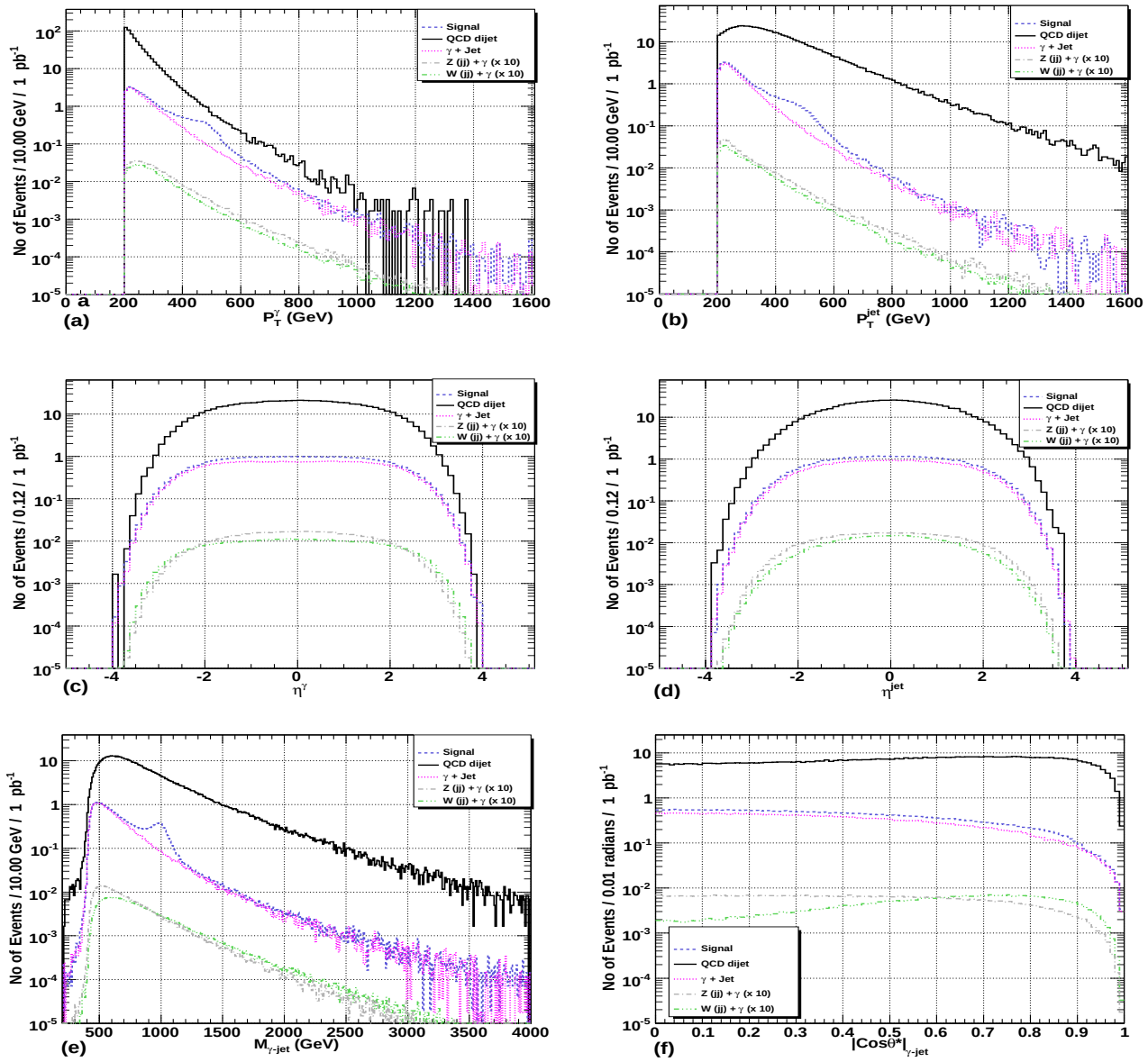

FIG. 7: Kinematic variable distributions after 200 GeV pre-selection cut on P_T (a) P_T^{γ} distribution (b) P_T^{jet} distribution (c) η^{γ} distribution (d) η^{jet} distribution (e) $M_{\gamma-jet}$ distribution and (f) $|\cos\theta^*|_{\gamma-jet}$. The signal corresponds to $M_{q^*} = 1\,\text{TeV}$.

partonic subprocess center of mass frame through

$$\eta(\gamma) = \frac{1}{2} ln\left(\frac{x_1}{x_2}\right) + \eta^*(\gamma)$$

where x_i are the momentum fractions of the incoming partons. For small $\hat{s}$ values (hence lower CKIN(3) cuts) the parton densities are maximized when the (anti-)quark acquire small(large) momentum fractions respectively. This leads to a considerably large contribution to η^{γ} from the boost, thereby smearing the original double peaked η^{γ} distribution into centrally peaked one. On the contrary, for typically high $\hat{s}$ (CKIN(3)$\geq$ 1 TeV) values the x_i tend to be not too different thereby reducing the smearing on this account.

In Table III we show the pre-selection efficiencies and geometrical acceptences for the CMS detector for various backgrounds and signal of M_{q^*} =1, 4 and 5 TeV against the total generated events.

VIII. ISOLATION VARIABLES

In a detector, a photon candidate is reconstructed by summing the electromagnetic energy deposition in ECAL towers in a limited region of space, with the sum being required to be above a certain E_T threshold. For the sake of simplicity, this limited region can be visualized as a cone in $\Delta\eta - \Delta\phi$ space given by $\Delta R \equiv \sqrt{\Delta\phi^2 + \Delta\eta^2}$, and containing most of the energy of the electromegnetic object.

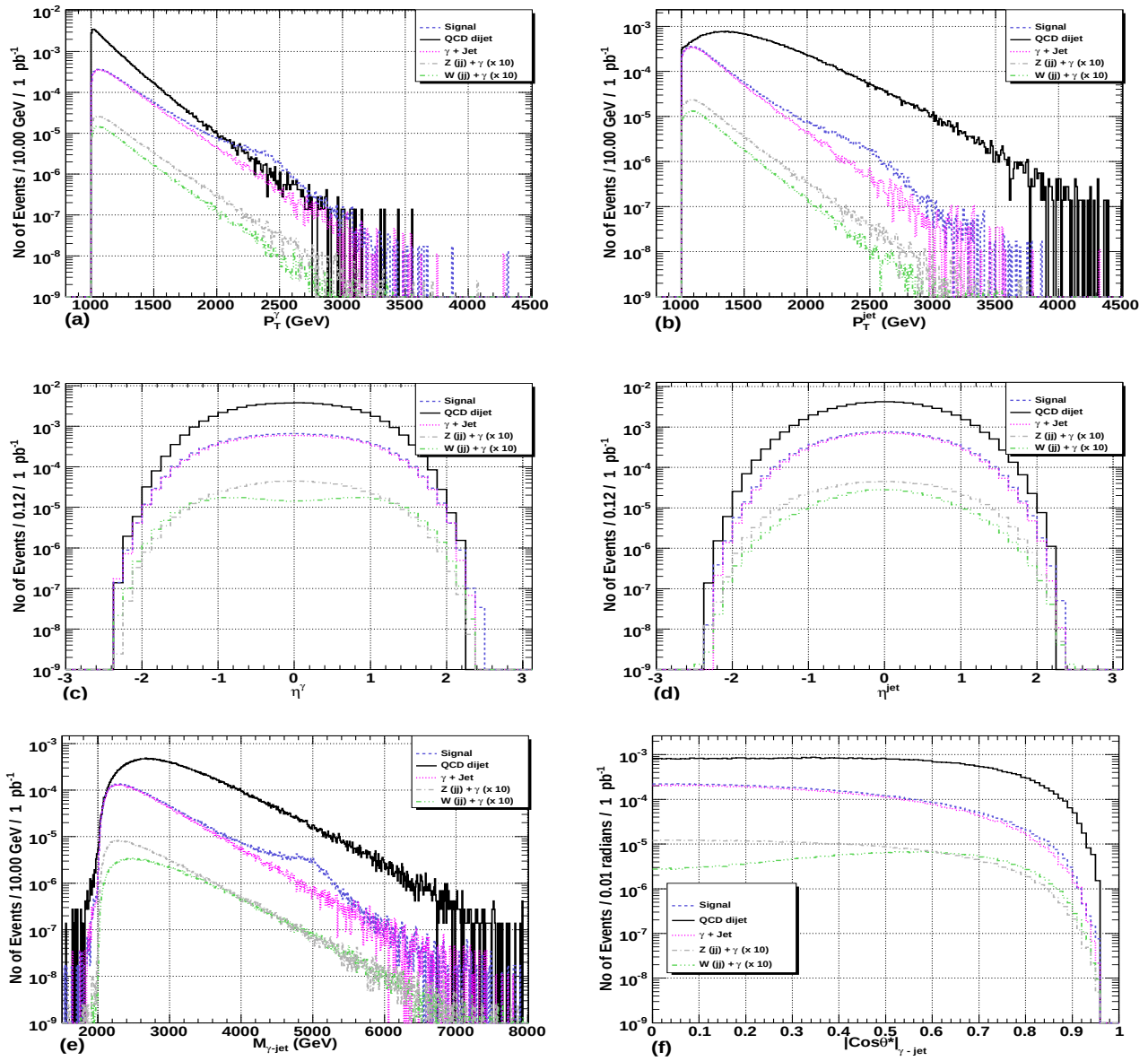

FIG. 8: As in Fig.7 but with a 1 TeV pre-selection cut on P_T and a signal corresponding to $M_{q^*} = 5\,\text{TeV}$ instead.

A jet fragmenting into neutral and charge hadrons with a $\pi^0 \to \gamma\gamma$ (with overlapping photons) carrying maximum momentum can also lead to fake single-photon candidates. To remove such events, photons are required not to have associated charged tracks within a cone of size $R_{\rm iso}$. This is implemented by requiring that the scalar/vector sum of energy/transverse momentum within $R_{\rm iso}$ should be below a certain threshold. For example, the DØ and the CDF experiments demand that the E_T due to charged tracks within a cone of $\Delta R = 0.4$ around the photon should be less than a certain value. In this anlaysis, we closely follow the CMS detector simulation studies [44] and consider the following isolation variables:

- the number of tracks (N_{trk}) above a certain threshold inside a cone around the photon candidate.
- the scalar sum of transverse energy (E_{TSUM}) inside a cone around the photon. Although, in a full detector simulation the E_{TSUM} is measured separately for ECAL and HCAL, but working at the generator level, we combine them into a single variable with all kinds of electromagnetic and hadronic objects around the photon being taken into account.

A. Track Isolation

For the purpose of track isolation, only 'stable' charged particles e.g. $\pi^{\pm}$, $K^{\pm}$, $e^{\pm}$ and $P^{\pm}$ were considered. The other particles were found to have only a negligible contribution. Indeed, $\pi^{\pm}$ alone contribute more than 80% of the charged tracks. Fig 9 shows the distribution of num-

ber of charged tracks (N_{trk}) around the leading photon within a cone of size $\Delta R \leq 0.35$ for a $M_{q^*} = 1$ TeV signal as well as for the total background. Since the leading photon is the *true* photon for signal events, most of them are associated with zero tracks (N_{trk} =0) and the distribution falls off very rapidly for larger N_{trk} values. For background events though, the distribution peaks at N_{trk} ∼7-8 and then falls slowly. The small rise at $N_{trk} = 0$ is due to the fact that $\gamma + jet$(SM) and $W/Z + \gamma$ backgrounds have true photons as the leading photon in the event and have no tracks around them, while the rising part along with the extended tail is mainly contributed by the QCD dijet events where the fake photon typically has a large number of tracks around itself. In this study, we accept a photon to be an isolated one if there is no track with minimum transverse momentum (P^{trk}_{Tmin}) within a given cone around it. It should be noted that comparative distributions of signal and total background, as shown in Fig 9, is not overly sensitive to moderate changes in the P^{trk}_{Tmin} value (the exact values are discussed at a later stage).

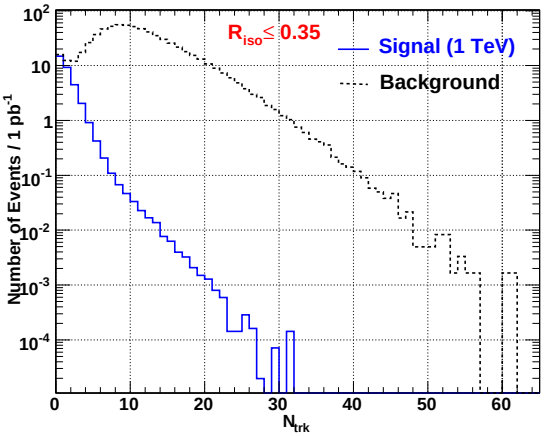

FIG. 9: Number of tracks(N_{trk}) for the signal (M_{q^*} =1 TeV) and the background events around the photon.

In pp collisions at the LHC, a large number of soft tracks (in the range of a few MeVs to a few GeVs) will be produced in each event. The main sources of such soft tracks are ISR, FSR, minimum bias and underlying events. For a direct photon emerging from the hard interaction, such soft tracks could actually be in the near vicinity of the photon. Labelling such photons as non-isolated ones could potentially reduce the signal efficiency, and many interesting events, such as those in this study, could be lost. To prevent such loss, tracks are usually required to pass certain minimum selection criteria, with a minumum threshold on the transverse momentum being a common requirement [29, 44, 45]. Adopting this strategy, we investigate the dependence of the signal efficiency and the signal/background (S/B) ratio on the chosen P_T threshold (P^{trk}_{Tmin}), varying the latter between 1-3 GeV.

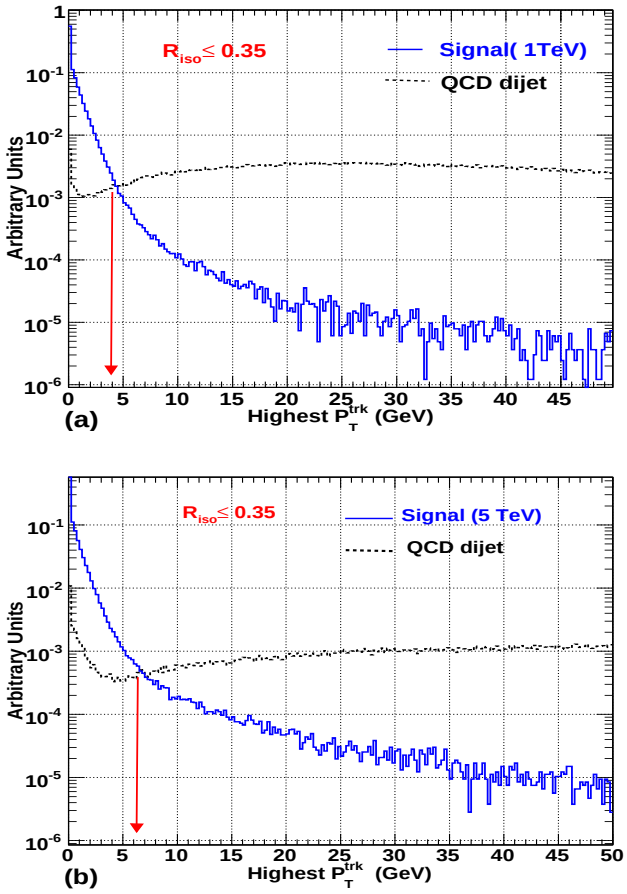

FIG. 10: Highest P_T track around leading photon for the signal and the QCD background a) M_{q^*} =1 TeV b) M_{q^*} =5 TeV. An isolation cone of size 0.35 has been used. Both distributions are normalized to unity for the sake of comparison. Note that the background differs between the two panels on account of the differing requirements on $\hat{P}_T$ (vide Sect.IV).

To optimize the value of P^{trk}_{Tmin}, it is useful to examine both the signal and the QCD dijet background in terms of the distribution for the highest-P_T track. In Fig 10(a) and (b) respectively, we display this distribution for the signal for $M_{q^*} = 1$ TeV and 5 TeV. Accompanying these, in each case, are the corresponding QCD dijet background. For ease of comparision both the distributions are nomralized to unity. As is evident, any tracks accompanying the photon in a signal event tend to have a low P_T, whereas for the background events, the distribution is a very wide one. An indicative value for the optimal P^{trk}_{Tmin} is given by the point of intersection of the two normalised distributions (signal and background). The optimal choice does depend on the signal profile (determined, in a large measure by the typical momentum transfers), as is evident from the crossover points being ∼4 (6) GeV for signals corresponding to M_{q^*} of 1 (5) TeV. Thus, characterizing only those tracks, around a photon, with a $P_T \gtrsim 4$ GeV as true tracks (or, in other words, accepting photons with accompanying tracks satisfying

$p_T \leq P^{trk}_{Tmin} \sim 4\,\mathrm{GeV}$ as true photons) would mean that a very large fraction of the signal is retained while a significant fraction of the background is rejected. In Fig. 11, we display the consequent interplay between signal efficiency and the signal to background ratio (S/B), for two different signal points (M_{q^*} =1 TeV and 5 TeV). It is evident from the distributions that adopting a higher threshold would remarkably increase the signal efficiency with only a small loss in the S/B ratio. More importantly, the track isolation requirement reduces the fake photon events with the major effect showing up in the QCD dijet background. As is obvious, the strict requirement of $N_{trk} = 0$ in a given cone around the photon reduces only a small fraction of the signal whereas the S/B ratio is improved considerably.

To keep the analysis simple, we then dispense with a M_{q^*}-dependent choice of the threshold, and instead demand P^{trk}_{Tmin} = 3 GeV and N_{trk} = 0 irrespective of the mass of the q^* being looked for. Although a choice of P^{trk}_{Tmin} = 4 GeV would have led to better results (see Fig 9), we make a more conservative choice to account for the fact that, in a real detector, the tracking efficiency is usually less than 100 %.

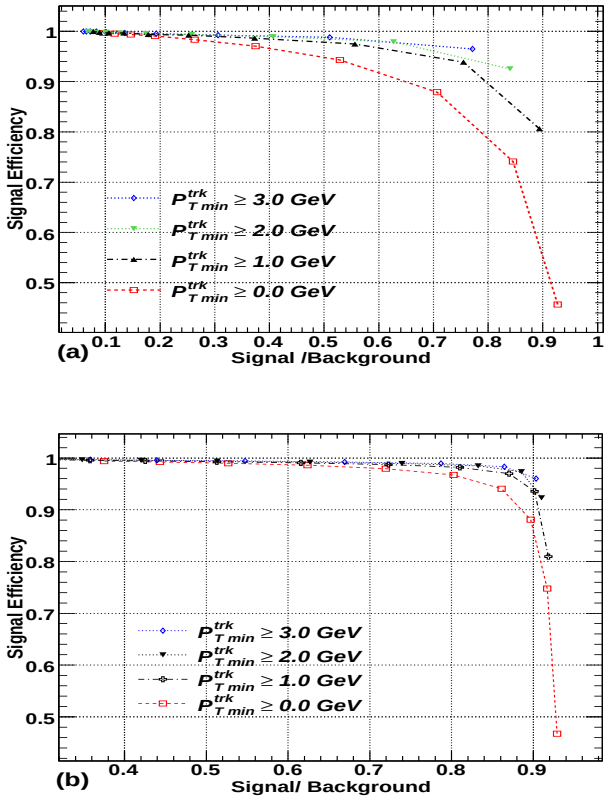

FIG. 11: Effect of P^{trk}_{Tmin} choice on signal efficiency vs S/B for the photons from a) 1 TeV signal b) 5 TeV signal. For a given threshold (P^{trk}_{Tmin}), the individual points correspond to differing values of the number of tracks, N_{trk}, allowed in a cone starting with 0 tracks (for the rightmost point) and increasing in steps of one.

B. E_T Sum Isolation

We now discuss the next isolation variable, namely the scalar sum of transverse energy inside a cone around the photon candidate. Figs.12a(b) show respectively the E_{TSUM} distribution for the leading photon for M_{q^*} = 1 (5) TeV for a cone of size $\Delta R = 0.35$. Both distributions are normalized for an integrated luminosity of $1\,\mathrm{pb}^{-1}$. It is evident that, in either case, a large fraction of signal events have $E_{TSUM} \leq 5.0\,\mathrm{GeV}$ whereas the background events generically have $E_{TSUM} \geq 5\,\mathrm{GeV}$. For $M_{q^*} = 5\,\mathrm{TeV}$, the discriminating point is even slightly higher.

As in the previous subsection, we next study the dependence of signal efficiency and S/B ratio on the choice of the E_{TSUM} threshold. Fig 13(a) and (b) respectively show the signal efficiency vs. S/B ratio for 1 TeV and 5 TeV signal points. It is evident that, for a given signal efficiency, a higher S/B ratio can be attained for larger cone sizes. For example, demanding $\Delta R \leq 0.35$ leads to a large signal efficiency ($\sim 92\%$) and $S/B > 0.88$ for either choices of M_{q^*}. On the other hand, any relaxation beyond $E_{TSUM} > 5.0\,\mathrm{GeV}$ reduces S/B considerably with only a very small gain in signal efficiency. Several E_{TSUM} thresholds for different cone sizes were analyzed along with track isolation requirements to optimize signal efficiency along with the S/B ratio.

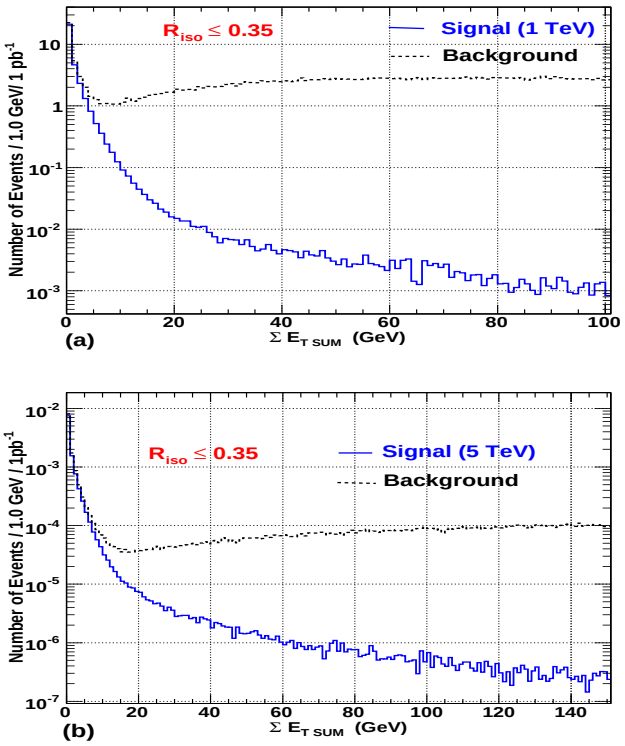

FIG. 12: E_{TSUM} for the background and the signal events around photons for a) M_{q^*} =1 TeV b) M_{q^*} =5 TeV Signal. Distributions are normalized for $\int Ldt = 1\,\mathrm{pb}^{-1}$.

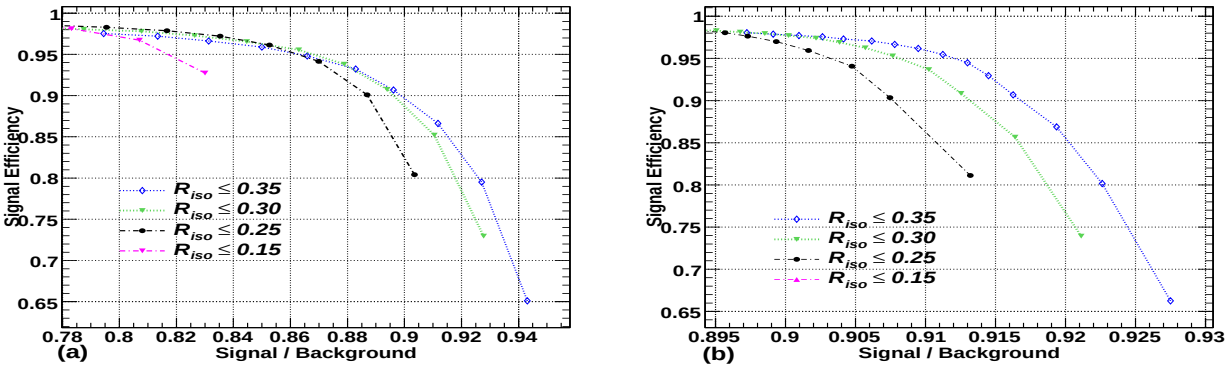

FIG. 13: Signal efficiency vs. S/B ratio for different cone sizes for different choices of the E_{TSUM} threshold around the leading photon for (a) M_{q^*} =1 TeV and (b) M_{q^*} = 5 TeV. For each choice of the cone size, individual points correspond to a particular choice for the E_{TSUM} threshold in that cone, starting with 1 GeV at the rightmost point and going up in steps of 1 GeV.

TABLE IV: Fraction of events surviving for the signal and various backgrounds for different isolation cuts (after P_T Cut).

R_{iso}	N_{trk}	P^{trk}_{Tmin} (GeV)	E^{max}_{TSUM} (GeV)	S (%)	QCD (%)	$\gamma + Jet$ (%)	$Z + \gamma$ (%)	$W + \gamma$ (%)	(S/B)
				M_{q^*} = 1.0 TeV					
0.30	0	1.0	5.0	73.6	0.93	72.9	75.0	71.9	0.970
			6.0	73.7	0.94	73.1	75.1	72.0	0.967
		2.0	5.0	81.2	1.12	80.6	82.9	79.4	0.951
			6.0	81.7	1.15	81.0	83.3	79.9	0.946
		3.0	5.0	83.0	1.19	82.3	84.8	81.2	0.941
			6.0	83.7	1.25	83.1	85.6	81.9	0.930
0.35	0	1.0	5.0	69.8	0.82	69.3	71.1	68.2	0.984
			6.0	70.1	0.83	69.5	71.4	68.5	0.982
		2.0	5.0	79.0	1.01	78.4	80.5	77.2	0.967
			6.0	79.8	1.05	79.1	81.4	78.0	0.960
		3.0	5.0	81.0	1.08	80.4	82.6	79.2	0.957
			6.0	82.2	1.14	81.6	83.9	80.4	0.947
				M_{q^*} = 5.0 TeV					
0.30	0	1.0	5.0	82.9	1.82	83.1	83.3	81.6	0.955
			6.0	83.1	1.83	83.2	83.5	81.8	0.954
		2.0	5.0	91.1	2.11	91.1	91.5	89.5	0.950
			6.0	91.5	2.14	91.6	91.9	89.9	0.950
		3.0	5.0	92.9	2.17	93.0	93.4	91.3	0.949
			6.0	93.7	2.22	93.7	94.2	92.1	0.947
0.35	0	1.0	5.0	78.8	1.63	79.0	79.3	77.7	0.960
			6.0	79.0	1.64	79.2	79.5	77.9	0.960
		2.0	5.0	88.6	1.94	88.7	89.0	87.2	0.956
			6.0	89.3	1.97	89.4	89.8	87.9	0.956
		3.0	5.0	90.6	1.99	90.7	91.1	89.2	0.955
			6.0	91.9	2.04	91.9	92.4	90.5	0.954

C. Final Selection Cuts

In Table IV, we show the efficiencies for signal and background for all the isolation variables with differing thresholds. Since we aim to observe any excess as a mass peak over the SM continuum and, in the early phase of the LHC operation, would be able to identify a signal only for low masses, it is rather important to have a large signal efficiency and S/B ratio for smaller M_{q^*}. Hence we have used the isolation criteria befitting a 1 TeV signal point (note that this also works reasonably for higher M_{q^*}s), and performed this analysis for all the different signal points considered in this study. Note that, while it is indeed possible to have yet other criteria to select different threshold based on real detector simulation, the

TABLE V: Number of events surviving for the $M_{q^*} = \Lambda$ =1 TeV signal and the backgrounds for $\int Ldt = 100pb^{-1}$ for different isolation cuts.

R_{iso}	N_{trk}	P^{trk}_{Tmin} (GeV)	E^{max}_{TSUM} (GeV)	S	QCD	$\gamma + Jet$	$Z + \gamma$	$W + \gamma$	Tot.Background	(S+B)
0.30	0	1.0	5.0	2734	626.2	2185	4.10	2.97	2818	3368
			6.0	2740	634.4	2190	4.11	2.98	2831	3381
		3.0	5.0	3085	803.0	2467	4.64	3.36	3278	3896
			6.0	3112	845.9	2490	4.68	3.39	3344	3966
0.35	0	1.0	5.0	2596	554.0	2076	3.89	2.82	2637	3157
			6.0	2604	560.8	2083	3.91	2.83	2650	3172
		3.0	5.0	3011	727.4	2409	4.52	3.28	3144	3747
			6.0	3054	772.1	2444	4.59	3.32	3224	3834

qualitative differences in the results are small.

Based on these studies, the final selection cuts applied are as follows (the $P_T^{\gamma,jet}$ requirements being determined by the range of M_{q^*} being investigated, vide Sect.IV):

- P_T^{γ}, $P_T^{jet} \geq 200$ GeV(500 GeV, 1 TeV);
- $|\eta^{\gamma}| \leq 2.5$ & $|\eta^{\gamma}| \notin [1.4442, 1.5666]$;
- $|\eta^{jet}| \leq 3.0$;
- $N_{trk} = 0$ for $P_T^{trk} \geq 3.0$ GeV within $R_{iso} \leq 0.35$;
- $E_{TSUM} < 5.0$ GeV within $R_{iso} \leq 0.35$.

In Table V, we show the expected number of events for $M_{q^*} = \Lambda = 1$ TeV for an integrated luminosity of 100 pb^{-1} for various combinations of isolation variables discussed above.

In Fig. 14 we have shown the invariant mass distribution for both signal+background(S+B) and background(B) after the all selection cuts.

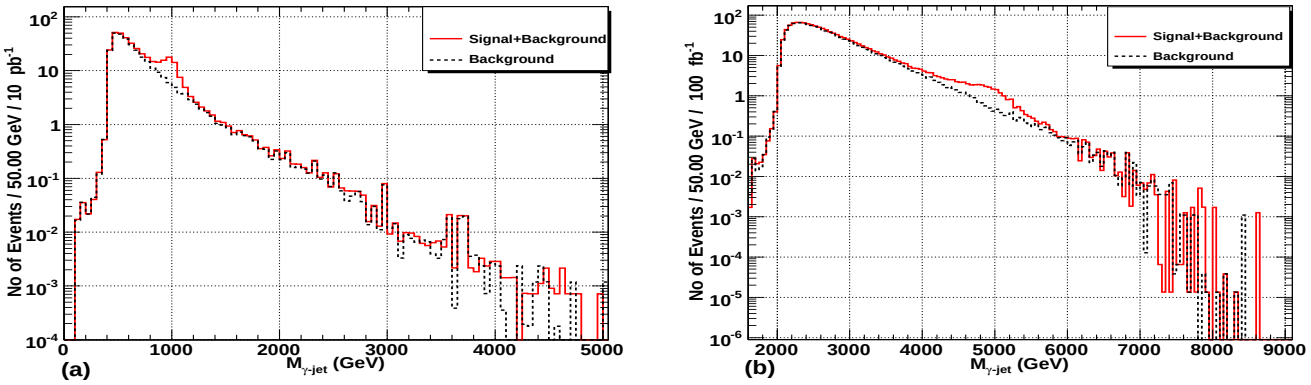

FIG. 14: Invariant mass of $\gamma-$jet system for Signal+Bacgkround and Background after all the isolation and kinematical cuts. (a) M_{q^*} = 1TeV (b) M_{q^*} = 5TeV.

IX. SIGNIFICANCE LEVEL

For reporting a discovery significance, we adopt a frequentist Monte-Carlo technique based on a method of hypothesis testing originally due to Neyman and Pearson [29, 46, 47]. The aim is to determine which one of two competing hypotheses, the so called null hypothesis(H_0) and the alternative hypothesis(H_1) is favoured by the data. In the present context, the SM only case (background) constitutes the null hypothesis (H_0) and the presence of new physics (i.e. excited quark contribution to the final state) alongwith the SM is the alternative hypothesis (H_1). Heretofore, H_0 and H_1 will also be referred to as background only (B) and signal plus background (S+B) hypotheses.

In the Neyman-Pearson method one aims to design a test which minimizes the probability β of erroneously rejecting an alternative hypothesis when it is actually true.

Understandably, $1-\beta$ is defined as the power of a test and the most powerful (MP) test is the one which maximizes the power for a given value of the probability α of rejecting the null hypothesis as false, when it is true instead. According to the Neyman Pearson lemma [46], the condition for the MP test is obtained as a condition on the log likelihood ratio (LLR) of a given dataset coming from the null or the alternative hypothesis. Even when a MP test does not exist, the LLR statistic can be used for testing between two hypothesis due to its statistically desirable properties [48]. One accepts or rejects H_0 based on the value of the LLR computed from the data. If the value of the LLR falls within a range of values (the critical region) which is unlikely to come from H_0 then H_0 is rejected. Now, α as defined above is clearly the probability of the LLR value falling in the critical region when H_0 is true. Hence, $1-\alpha$ is reported as the significance level of rejecting H_0 (i.e., the SM in our case), or, in other words, this is the discovery confidence level.

In general, a LLR test can be constructed out of one or many discriminating quantities (e.g. P_T, angular separation etc.). In this analysis, the LLR has been constructed out of a single discriminating variable, namely $M_{\gamma-jet}$, the invariant mass of the leading γ and jet. While this is obviously the most sensitive discriminant in the case of on-shell production, it plays an important role even for virtual exchanges[31].

The likelihood ratio is defined as the ratio of Poisson probabilities:

$$\begin{aligned} Q &= \frac{P_{poiss}(data|S+B)}{P_{poiss}(data|B)} \\ P_{poiss}(data|S+B) &\equiv \frac{(s_i+b_i)^{n_i}e^{-(s_i+b_i)}}{n_i!} \\ P_{poiss}(data|B) &\equiv \frac{(b_i)^{n_i}e^{-(b_i)}}{n_i!} \end{aligned} \qquad (7)$$

where s_i+b_i are the number of events expected in the $i^{\rm th}$ bin of the $M_{\gamma-jet}$ histogram according to the S+B hypothesis whereas b_i correspond to the B hypothesis. n_i here denote the number of events in the $i^{\rm th}$ bin of $M_{\gamma-jet}$ histogram from "*data*". All efficiencies are to be folded in s_i, b_i and n_i.

The LLR statistic is then given by the expression,

$$-2\ln Q = 2\sum_{i=1}^{n_{bins}} s_i - 2\sum_{i=1}^{n_{bins}} n_i \ln\left(1+\frac{s_i}{b_i}\right) \qquad (8)$$

The "*data*" n_i in the i^{th} bin of the test variable is generated as a random Poisson fluctuation around the mean value of the i^{th} bin of the theoretical $M_{\gamma-jet}$ histogram.

The significance level is defined as,

$$\alpha = 1 - CL_B = P(Q \le Q_{obs}|B), \qquad (9)$$

the fraction of experiments in a large ensemble of background only experiments which would produce results more signal-like than the observed data. By definition, a S+B hypothesis is "confirmed" at the 5σ (3σ) level if α<$2.8\times10^{-7}(1.35\times10^{-3})$ [49].

In Fig. 15, we show the LLR distribution for B and S+B type hypotheses for two different mass points. The luminosities have been chosen so as to yield a 5σ significance for the S+B hypothesis. We have used 10^7 MC trials for these distributions. In this figure, $1-CL_B$ is the fraction of MC trials of background type hypothesis which falls to the left side of peak value of LLR_{S+B}.

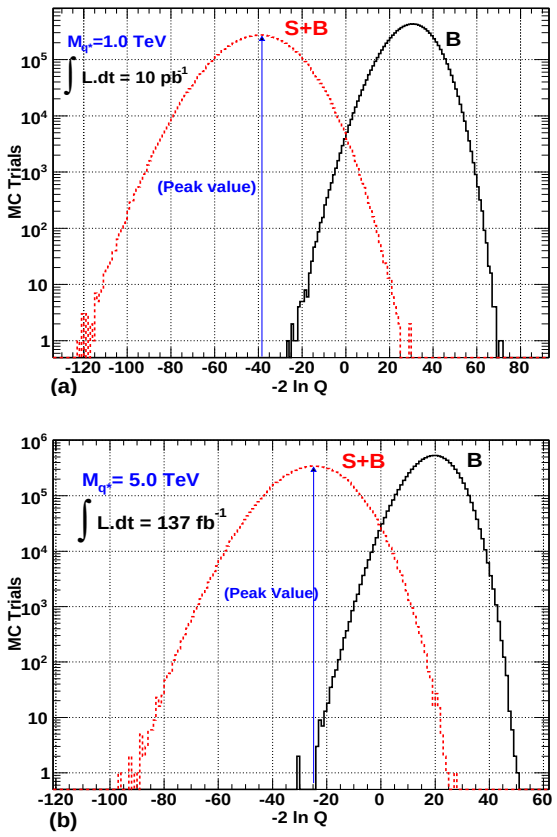

FIG. 15: Log likelihood ratio distributions for S+B and B type hypotheses for a $5\sigma-$significance for (a) 1.0 TeV (b) 5.0 TeV q^* states.

In Fig. 16 we show how the LLR discrimination between two types of hypothesis behave as a function of mass window around the M_{q^*} value. As visible from the figure, beyond $\pm3\Gamma(q*)$ the two hypthesis looks similar and hence it does not contribute to the significance level. We found similar results for all signal points and for the final selection we have used $\pm3\Gamma(q*)$ as the mass window around $\gamma-jet$ invariant mass.

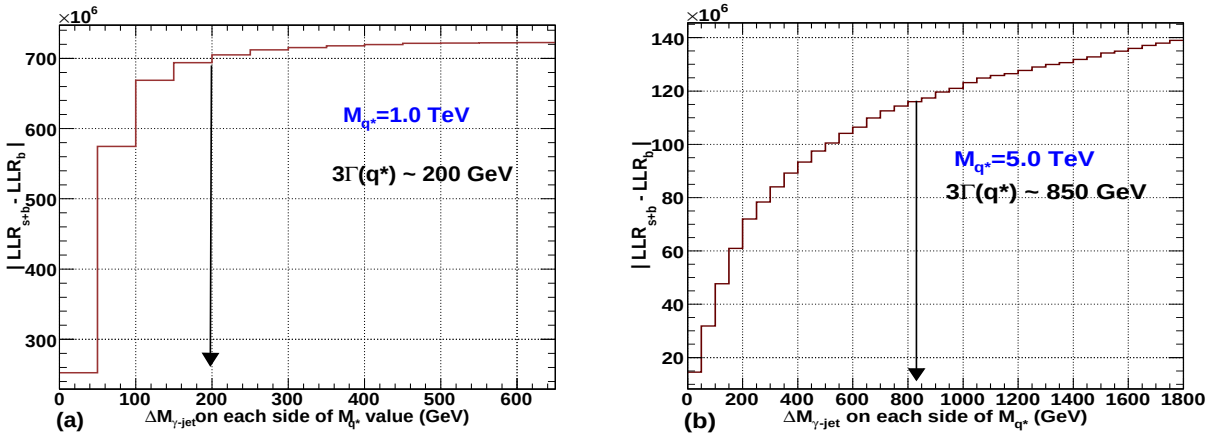

FIG. 16: Effective LLR contribution as a function of $\Delta M_{\gamma-jet}$ on each side of q^* state of mass (a) 1.0 TeV and (b) 5.0 TeV.

X. BACKGROUND SUBTRACTED INVARIANT MASS

In this section, we describe a procedure to estimate the number of events under the mass peak in the case of a discovery (i.e. if the data supports the S+B hypothesis). Assuming an excess centred aproximately around $M_{\gamma-\mathrm{jet}} = M_0$, the first step constitutes fitting the data over a $M_{\gamma-\mathrm{jet}}$ range centred around M_0 but much wider than the region of the excess, the aim being to fit the background as well as the sidebands. While in a real experiment one would attempt to fit the sidebands from data alone, here we use a large MC sample to determine the shape of the sidebands and find that an exponential describes them well (see Fig. 17 for $M_0 = 1\,\mathrm{TeV}$). To generate realistic distributions, we consider (s + b) in each bin to be an independent Poisson distributed (and integer valued) variable with a mean equalling the theoretically expected number of events. A random fluctation was then used to generate the "experimentally observed" events in the bin concerned. For a good background fit on the (S+B) distribution, an identified excess has clearly to be left out. To this end, we leave out the range $\sim [M_0 - 3\,\Gamma_0, M_0 + 3\,\Gamma_0]$ consonant with the binning algorithm where $\Gamma_0 = \Gamma(M_{q^*} = M_0)$. For a χ^2 minimization of the fit, the MINUIT [50] package was used within the *ROOT* framework [51]. The fit in Fig. 17(a) was done for an integrated luminosity of $1\,\mathrm{fb}^{-1}$ although a 5σ signal significance for $M_{q^*} = 1\,\mathrm{TeV}$ is attainable with only $10\,\mathrm{pb}^{-1}$ of data. Fig 17(b) shows the background subtracted mass distribution for M_{q^*} =1 TeV. Here we have used a single Gaussian to fit the mass spectrum.

While an integrated luminosity of $1\,\mathrm{fb}^{-1}$ for new physics mass measurements would normally be considered meagre when compared to the LHC design parameters, it is interesting to consider the physics possibilities with far lower luminosities. To this end, we present, in Fig 18, analogous distributions for only $10\,\mathrm{pb}^{-1}$. While

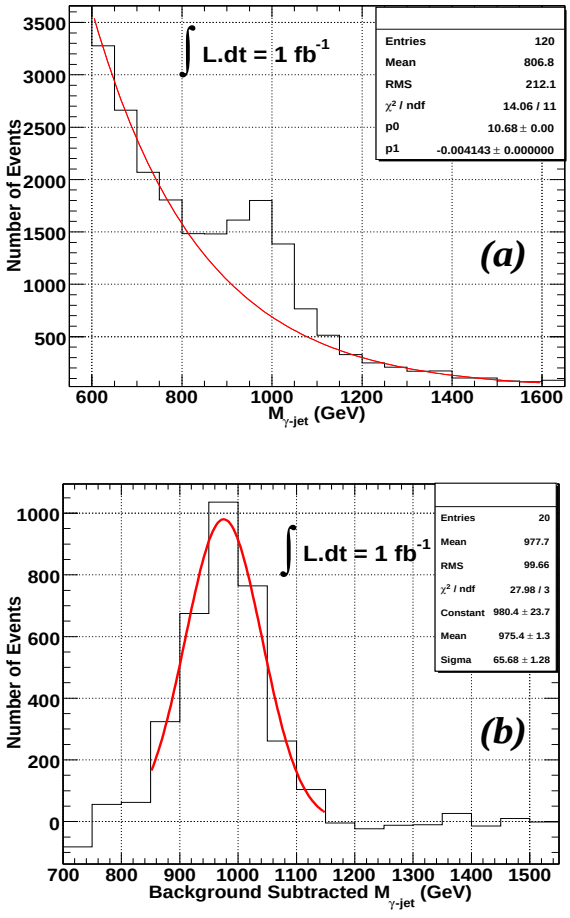

FIG. 17: (a)Background fit on the (S+B) distribution with an exponential function for 1.0 TeV q^* for an integrated luminosity of $1\,\mathrm{fb}^{-1}$. (b) The corresponding background subtracted invariant mass distribution.

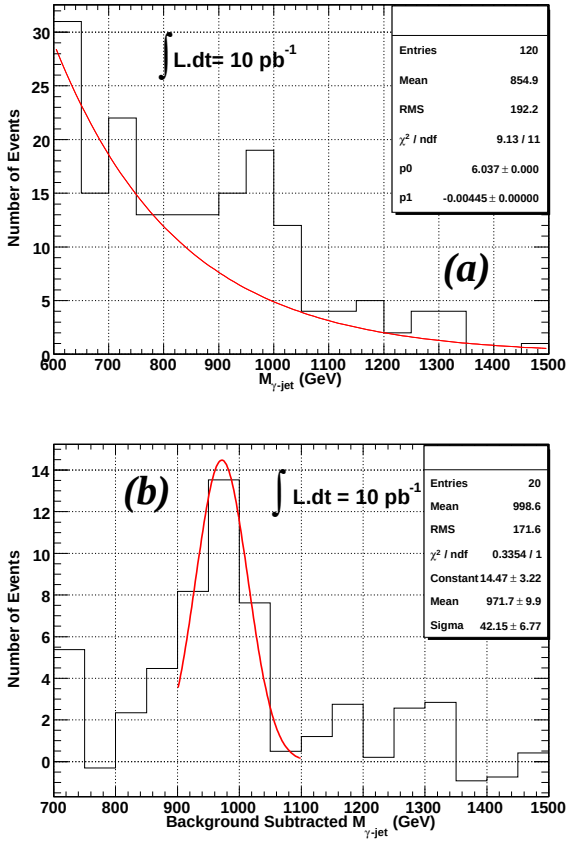

FIG. 18: As in Fig.17, but for an integrated luminosity of $10\,\mathrm{pb}^{-1}$ instead.

the fit for the background is, understandably, not as good as in the earlier case, once the validity of an exponential fit is accepted, the background subtracted mass fit is still very convincing. In Fig 18(b) the number of signal events under the Gaussian fit and within the 800–1200 GeV mass range was found to be $30.5 \pm 5.5(stat.)$. The uncertainty due to error on fitting parameters are found to be at most 4.9 events.

We note in passing that in an actual detector at the LHC the mass peak will have a tail on the lower mass side due to partial containment of showers and fitting this may need a Gaussian modified with a Landau or some other asymmetric distribution thereby broadening the mass peak somewhat.

The invariant mass distribution has two components, the natural Lorentzian part for an unstable particle with a large width and a Gaussian (or a double-Gaussian) distribution due to resolution effects. The combined distribution is a convolution of the two above. Although the combined distribution is thus not a simple one, a single Gaussian fits the mass peak reasonably well and hence we choose to fit the peak with a simple Gaussian.

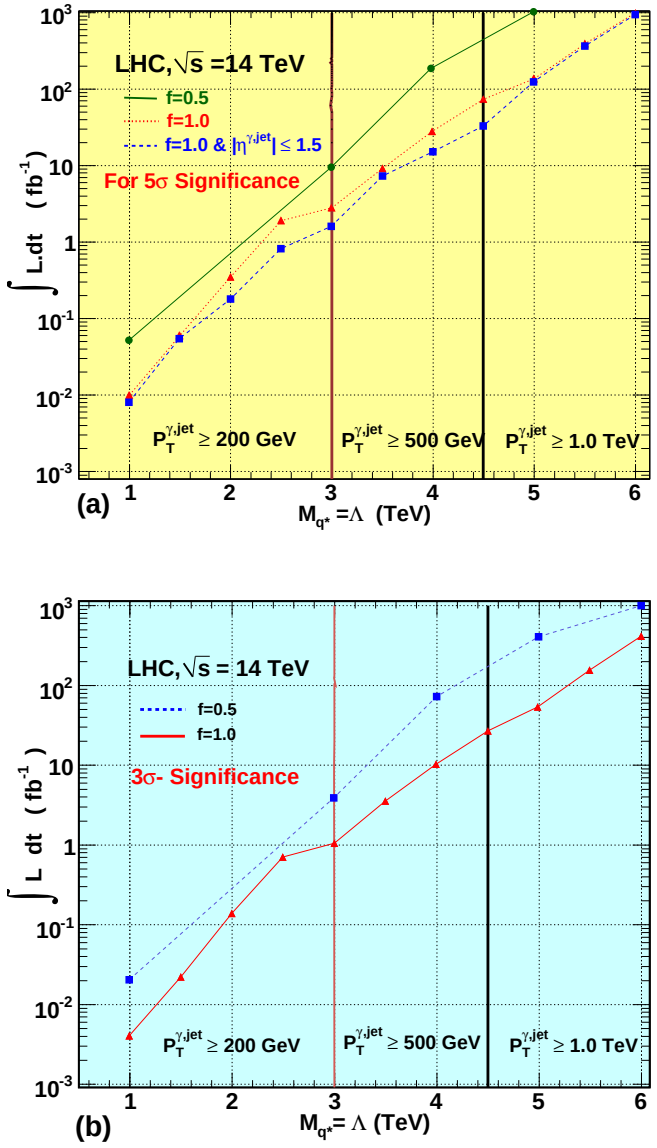

FIG. 19: Required integrated luminosity as a function of M_{q^*} for (a) 5σ and (b) 3σ significance for two different coupling strengths (systematic uncertainties are not included).

XI. RESULTS

Fig. 19(a) and (b) respectively show the luminosity needed to achieve 5σ (3σ) significance for the signal as a function of the excited quark mass. We find that the result obtained using $(-2\,\ln Q)$ are consistent with those from $s/\sqrt{b}$ test statistic. In estimating the required luminosity, we have exploited only the mass peak region of the signal over the SM background. We have used a mass window of $\sim \pm 3\Gamma(q*)$ around M_{q^*}. In a previous section we have shown that beyond $\pm 3\Gamma(q*)$ the discriminating statistic, namely LLR, looks similar for S+B and B.

We have checked the stability of the results by varying

TABLE VI: Cross sections for various M_{q^*} values after imposing all kinematical and isolation cuts.

S.N.	M_{q^*} [a] (TeV)	$\Delta M_{\gamma-j}$ $\pm 3\Gamma(q*)$ (GeV)	$\sigma(S+B)$ (pb)	$\sigma(B)$ (pb)	$\sigma(S^*)$ [b] (pb)	Efficiency(S+B) (%)	Efficiency(B) (%)	Efficiency(S*) (%)
1	1.0	800-1200	9.26	4.92	4.34	1.304	0.699	60.28
2	1.5	1200-1800	2.034	1.33	0.694	0.288	0.190	46.71
3	2.0	1600-2400	6.72×10^{-1}	5.10×10^{-1}	1.61×10^{-1}	0.095	0.072	37.23
4	2.5	2000-3000	2.54×10^{-1}	2.10×10^{-1}	4.41×10^{-2}	0.036	0.029	40.67
5	3.0	2450-3550	7.85×10^{-2}	6.44×10^{-2}	1.40×10^{-2}	0.011	0.009	75.95
6	3.5	2900-4150	1.11×10^{-2}	6.93×10^{-3}	4.17×10^{-3}	0.274	0.172	24.70
7	4.0	3300-4700	4.90×10^{-3}	3.40×10^{-3}	1.50×10^{-3}	0.121	0.084	15.60
8	4.5	3700-5300	2.20×10^{-3}	1.57×10^{-3}	6.37×10^{-4}	0.054	0.039	11.48
9	5.0	4150-5850	4.60×10^{-4}	2.47×10^{-4}	2.12×10^{-4}	0.628	0.342	22.49
10	5.5	4500-6450	2.17×10^{-4}	1.29×10^{-4}	8.81×10^{-5}	0.299	0.179	14.91
11	6.0	5000-7000	8.39×10^{-5}	5.14×10^{-5}	3.24×10^{-5}	0.115	0.071	7.85

[a]Here $f_1 = f_3 = 1.0$
[b]Pure New Physics contribution evaluated by subtracting B from $(S+B)$

TABLE VII: As in Table.VI with additional requirement of centrality ($|\eta^{\gamma,jet}| \leq 1.5$).

S.N.	M_{q^*} [a] (TeV)	$\Delta M_{\gamma-j}$ $\pm 3\Gamma(q*)$ (GeV)	$\sigma(S+B)$ (pb)	$\sigma(B)$ (pb)	$\sigma(S^*)$ [b] (pb)	Efficiency(S+B) (%)	Efficiency(B) (%)	Efficiency(S*) (%)
1	1.0	800-1200	4.75	2.14	2.61	0.668	0.304	36.22
2	1.5	1200-1800	0.87	0.41	0.45	0.123	0.059	30.64
3	2.0	1600-2400	2.27×10^{-1}	1.10×10^{-1}	1.16×10^{-1}	0.032	0.015	26.82
4	2.5	2000-3000	6.54×10^{-2}	3.43×10^{-2}	3.11×10^{-2}	0.009	0.004	28.66
5	3.0	2450-3550	2.21×10^{-2}	1.27×10^{-2}	9.40×10^{-3}	0.003	0.001	50.95
6	3.5	2900-4150	6.67×10^{-3}	3.20×10^{-3}	3.47×10^{-3}	0.165	0.079	20.55
7	4.0	3300-4700	2.64×10^{-3}	1.30×10^{-3}	1.34×10^{-3}	0.065	0.032	13.93
8	4.5	3700-5300	1.01×10^{-3}	4.59×10^{-4}	5.51×10^{-4}	0.025	0.011	9.92
9	5.0	4150-5850	3.99×10^{-4}	2.00×10^{-4}	1.98×10^{-4}	0.545	0.277	20.98
10	5.5	4500-6450	1.79×10^{-4}	9.78×10^{-5}	8.15×10^{-5}	0.246	0.135	13.78
11	6.0	5000-7000	6.51×10^{-5}	3.44×10^{-5}	3.07×10^{-5}	0.089	0.047	7.43

[a]Here $f_1 = f_3 = 1.0$
[b]Pure New Physics contribution evaluated by subtracting B from (S+B)

the bin width of the invariant mass distribution from 50 GeV to 20 GeV for both $M_{q^*} = 1.0\,\text{TeV}$ and 2.0 TeV and find that the luminosity required for 5σ significance changes by 20% and 1.1 % respectively. For $M_{q^*} = 5.0\,\text{TeV}$, on the other hand, we varied the bin width from 50 GeV to 100 GeV and found that the required luminosity changes by 2.1 %. Similarly we increased the number of Monte Carlo trials by a factor of 10 and found that the required luminosity changes by $\sim$ 20 %, 0.8 % and 2.1 % respectively for the 1.0, 2.0 and 5.0 TeV mass points.

In Fig. 19(a), corresponding to the $f_i = 1.0$ case, we also demonstrate the effect of restricting the photon and the jet to the central region of the calorimeter on the required luminosity. For 5σ significance, the latter reduces by $\sim 30\%$ upto a mass of 4.5 TeV. For $M_{q^*} \gtrsim 5.0\,\text{TeV}$, though, the signal events are mostly produced in the central region and hence the requirement $|\eta^{\gamma,jet}| \leq 1.5$ does not affect the final result significantly. It is also shown that within the present model of compositenes for $M_{q^*} \gtrsim 5.5\,\text{TeV}$, a 5σ significance can not be achieved at a centre of mass energy of 14 TeV. While this might seem to run counter to previous work, note that, unlike in the earlier efforts, we have used unitarized amplitudes and hence our cross sections are naturally smaller than theirs.

In Table VI, we show the results for cross section and efficiency for S+B and B after all the kinematical and isolation selection cuts have been imposed for various M_{q^*} values. Tabel VII shows similar information for central events alone ($|\eta^{\gamma,jet}| \leq 1.5$).

XII. SYSTEMATIC UNCERTAINTIES

Since we have performed a detailed analysis including a realistic simulation of various detector effects and uncertainties for the CMS setup, here we present an es-

timation of systematic uncertainties. For this we have considered only the dominant contribution both in the signal and the backgrounds. For both the signal and the $\gamma + jet$ background we concentrate on the dominant process, viz. $qg \to q\gamma$. For the QCD dijet background, all the available processes in PYTHIA were used for the estimation of the uncertainty. We did not account for $q\bar{q} \to \gamma + jet$,$W/Z(jj) + \gamma$ and $gg \to \gamma + jet$ as they contribute only a small fraction of the total background and systematic uncertainities in these can safely be neglected.

- Choice of the parton distributions (PDF): To estimate the uncertainty in the cross sections due to the choice of the PDF, the former were recalculated for three additional PDFs, namely CTEQ6L, CTEQ6M [52] and MRST2001 [53]. Using the LHApdf package [54], the results for each were compared to those for our default choice, namely CTEQ5L [27]. While the resultant cross sections turned out to be higher for CTEQ6M (it should be noted that the CTEQ6M distributions are NLO and hence their use with LO calculations is fraught with danger) and MRST2001 distributions, for CTEQ6L they turned out to be lower for almost all the signal points. As can be expected, the uncertainty in the cross section increases with M_{q^*}, simply because one starts to sample an ill-explored region in the (Q^2, x) plane. For CTEQ6M and MRST2001, the relative deviation varies between 2.3–13.0 % and 2.6–14.2 % respectively as M_{q^*} changes from 1 TeV to 6 TeV. For CTEQ6L, the variation was found to be within -4.5 to $+2.25$ %. These numbers are quite consistent with those applicable for the SM γ + jet process alone, for which the corresponding numbers are 5.6–11.0% (CTEQ6M) and 6.0-12.0%(MRS2001). Similarly, for the dijet background an uncertatinty of 9–16% (CTEQ6M) and 8.7–16.5% (MRST2001) was estimated.

  We have not only used different PDFs but have also evaluated uncertainty due to a given proton PDF by varying the errors on the parameters of the PDF fit itself. For this, we chose CTEQ6L (with NLO α_s and LO fit) and its 40 subset PDFs. The uncerainty was found to be $\sim \pm$ 1% for a 1 TeV q^* state and -8.29% to $+10.93\%$ for a 5 TeV one. For QCD di-jet and $\gamma + Jet$ background these numbers were found to be -9.81% to $+13.74\%$ and -8.04% to $+10.54\%$ respectively.

- Scale Variation: To estimate the dependence of the signal and the background cross-sections on the choice of the factorization scale Q (default value in our analysis being $\sqrt{\hat{s}}$), they were recalculated for two other values of the latter viz $Q^2 = P_T^2$ and $Q^2 = -\hat{t}$. Both these choices for the scale would have resulted in a higher cross-section compared to $Q^2 = \hat{s}$. The deviation increases with M_{q^*} and ranges between 2.1–11.3% for $Q^2 = -\hat{t}$ and 10.6–25.0% for $Q^2 = P_T^2$ case. For the QCD di-jet background the maximum deviation was found to be $\sim$39 % while for $\gamma + jet$ it was $\sim$26 %. Thus, the overall significance of the signal remains largely unaltered.

- Higher-order effects: For the background, these have been studied in detail both theoretically and experimentally. For example, $\gamma + jet$ production in the SM has been studied in depth using the NLO parton level Monte Carlo program JETPHOX [55, 56]. Recently, a comparison of these predictions have been done with the Tevatron data[57]. Unfortunately, the P_T^γ-dependent shape of the triple differential cross section$(d^3\sigma/dp_T^\gamma dy^\gamma dy^{jet})$ for different pseudorapidity ranges is not explained satisfactorily by the NLO calculation. The reason is not hard to fathom. A comparison with data necessitates the imposition of isolation cuts. On the other hand, the NLO calculations depend crucially on the choice of isolation cuts and infrared safety needs to be taken care of. This has been discussed in Ref.[58]. Modulo such subtleties, an effective and easy way to incorporate higher order effects is to include K-factors. For $\gamma + jet$ production, the K-factor lies in the range 1.0–1.66 depending on the details of jet fragmentation (primarily, to a γ/π^0)[59]. While the K-factor for our case is not known, in the large M_{q^*} limit it is not expected to be too different from the SM case. Close to threshold, the K-factor is normally expected to be even bigger. However, given the attendant theoretical complications, we adopt a conservative approach and ignore all K-factors in this analysis.

- Jet energy resolution: To incorporate finite detector resolutions, the photon and jet four momenta were smeared with a energy resolution as given in section VI. For the photon P_T range considered in this analysis, we expect the constant term (C) to be the dominant source of error and it contributes about 0.55%. To estimate the effect of the jet energy resolution on this analysis, we redid this analysis smearing the four momenta of the jet with an energy resolution of 100% for the barrel region and 150 % for the endcaps and the forward regions. The effect was studied for two different mass state, viz. 1.0 TeV and 5.0 TeV. It was found that such a large worsening of the jet energy resolution would increase the luminosity required for a 5σ significance by about 30% (1%) for 1.0 TeV (5.0 TeV) mass states respectively. However, if we increase the number of MC trials by a factor of 10 (to stablize the peak value of LLR_{S+B}) then these numbers were found to be well within 2%.

- Uncertainty due to pre-selection: The systematic uncertainty due to preselection in the P_T range of this study is found to be less than 1%.

- Luminosity error: For the CMS experiment, this error is expected to be $\sim 10\%$ for an integrated luminosity of $1\,\mathrm{fb}^{-1}$ [60] and $\sim 3\%$ for an integrated luminosity of $30\,\mathrm{fb}^{-1}$ [61].

- To estimate the combined effect of the aforementioned uncertatinties we lowered the signal cross-section by 5% for the 5.0 TeV mass point and found that the luminosity for 5σ significance increases by $\sim$ 10.9%. On the other hand, if we increase the background cross-section by 5% for the same mass point then the required luminosity increases by $\sim 5.1\%$.

XIII. CONCLUSIONS

To summarise, we have investigated the potential of using a direct photon (in association with a single hard jet) final state at the LHC to probe possible quark excitations. Such states arise naturally in a variety of scenarios, ranging from Kaluza-Klein excitations in extra-dimensional models to theories wherein the quarks themselves are composed of more fundamental objects (preons). And, as far as the concerns of the present analysis go, even other fundamental quarks (as often appear in theories with extended symmetries, gauged or global) could lead to similar signals and, hence, be discoverable.

In any such model, the excited states may couple to their SM counterparts only through a generalised (chromo-)magnetic transition term in an effective Lagrangian. Consequently, the presence of such states would alter the direct photon cross section, whether through an on-shell production (and subsequent decay) of the q^* or through an off-shell exchange (both s- and t-channel). The extent of the deviation depends on both the mass M_{q^*} and the compositeness/excitation scale Λ. The deviation concentrates in the large p_T regime, especially for larger M_{q^*} and can be quite substantial.

Two points need to be noted here. The first and straightforward one relates to the width of the excited state. With $\Gamma(q^*)$ being typically quite large, a narrow-width approximation does not hold and the full matrix element needs to be incorporated. The second issue is more subtle and is connected to the non-renormalizable nature of the effective Lagrangian. Since a naive use of a (chromo-)magnetic dipole moment vertex leads to a cross section constant or even growing with the center of mass energy, the amplitude needs to be unitarized. This, understandably, leads to a suppression of the cross sections, a fact often ignored in experimental analyses, but included here.

Using the photon and jet reconstruction algorithms as used for the CMS dectector at the LHC, we have performed a realistic estimation of the deviation caused by the excited quark exchange contribution to the direct photon plus a single hard jet rate. We have accounted for all major backgrounds to evaluate the limits in the $\Lambda - M_{q^*}$ parameter space. With the imposition of moderate restrictions on the rapidities (as dictated by the detector acceptances), but stringent cuts on the transverse momenta, the background can be beaten down severely without any damaging loss of signal. A most crucial ingredient is the application of reasonably stringent isolation criteria, as it helps control the orders of magnitude larger backgrounds from QCD dijet production with one jet faking a photon. The consequent exclusion limits that may be reached are very strong. While it may seem that these are still not as strong as some quoted in the literature, it should be realised that most of the latter have worked with a non-unitarised cross section and hence the two cannot be compared directly.

Acknowledgments

BCC would like to thank S. Mrenna for discussions on $W\gamma$ production. SB and DC acknowledge support from the Department of Science and Technology(DST), India under project number SR/S2/RFHEP-05/2006. BCC acknowledges support from the DST, India under project number SP/S2/K-25/96-V. SSC would like to express gratitude to the Council of Scientific and Industrial Research, India for financial assistance and to Prof. R.K. Shivpuri and Prof. Raghuvir Singh for support and encouragement.

[1] H. Harari and N. Seiberg, Phys. Lett. **B 98** (1981) 269;
M.E. Peskin, *in proceedings of the 1981 International Symposium on Lepton and Photon Interaction at High Energy,* W.Pfeil, ed., p880 (Bonn, 1981);
L. Lyons, Oxford University Publication 52/82 (June 1982).

[2] G. 't Hooft, in *Recent Developments in Gauge Theories*, G. 't Hooft *et al.*, eds. (Plenum Press, New York,1980).

[3] J.C. Pati, A. Salam and J.A. Strathdee Phys. Lett. **B 59** (1975) 265;
H. Fritzsch and G. Mandelbaum, Phys. Lett. **B 102** (1981) 319;
W. Buchmuller, R.D. Peccei and T. Yanagida, Phys. Lett. **B 124** (1983) 67; Nucl. Phys. **B 227** (1983) 503; Nucl. Phys. **B 237** (1984) 53;
U. Baur and H. Fritzsch, Phys. Lett. **B 134** (1984) 105;
X. Li and R.E. Marshak, Nucl. Phys. **B 268** (1986) 383;
I. Bars, J.F. Gunion and M. Kwan, Nucl. Phys. **B 269** (1986) 421;
G. Domokos and S. Kovesi-Domokos, Phys. Lett. **B 266** (1991) 87;
J.L. Rosner and D.E. Soper, Phys. Rev. **D 45** (1992) 3206;
M.A. Luty and R.N. Mohapatra, Phys. Lett. **B 396**

(1997) 161 [hep-ph/9611343];
K. Hagiwara, K. Hikasa and M. Tanabashi, Phys. Rev. **D 66** (2002) 010001; Phys. Lett. **B 592** (2004) 1.
[4] For a review and additional references, see R.R. Volkas and G.C. Joshi, Phys. Rep. **159** (1988) 303.
[5] K. Hagiwara, S. Komamiya and D. Zeppenfeld, Z. Phys. **C 29** (1985) 115;
U. Baur, M. Spira, and P.M. Zerwas, Phys. Rev. **D 42** (1990) 815;
F. Boudjema, A. Djouadi and J.L. Kneur, Z. Phys. **C 57** (1993) 425.
[6] ALEPH Collaboration, Phys. Lett. **B 385** (1996) 445; *ibid* **B 384** (1996) 439; *ibid* **B 250** (1990) 172; *ibid* **B 236** (1990) 501; *ibid* **B 236** (1990) 511;
DELPHI Collaboration, Phys. Lett. **B 393** (1997) 245; Zeit. Phys. **C 74** (1997) 57; *ibid* **C 74** (1997) 577; *ibid* **C 53** (1992) 41; Phys. Lett. **B 274** (1992) 230; *ibid* **B 380** (1996) 480; Eur. Phys. J. C **8**, 41 (1999);
L3 Collaboration, Phys. Lett. **B 412** (1997) 189; *ibid* **B 401** (1997) 139; *ibid* **B 377** (1996) 304; *ibid* **B 370** (1996) 211; *ibid* **B 295** (1992) 371; *ibid* **B 251** (1990) 321; *ibid* **B 247** (1990) 177; *ibid* **B 250** (1990) 205; *ibid* **B 252** (1990) 525; *ibid* **B 502** (2001) 37;
OPAL Collaboration, Eur. Phys. J. **C 1** (1998) 45; Phys. Lett. **B 393** (1997) 217; *ibid* **B 391** (1997) 197; *ibid* **B 386** (1996) 463; *ibid* **B 385** (1996) 433; Z. Phys. **C 52** (1991) 175; Phys. Lett. **B 257** (1991) 531; *ibid* **B 247** (1990) 448; *ibid* **B 244** (1990) 135; *ibid* **B 240** (1990) 250.
[7] H1 Collab., I. Abt *et al.*, Nucl. Phys. **B 396** (1993) 3;
H1 Collab., C. Adloff *et al.*, Phys. Lett. **B 525** (2002) 9;
H1 Collab., C. Adloff *et al.*, Phys. Lett. **B 548** (2002) 35;
H1 Collab. C. Adloff *et al.*, Eur. Phys. J. **C 17** (2000) 567;
ZEUS Collab., M. Derrick *et al.*, Z. Phys. **C 65** (1994) 627;
ZEUS Collab., S. Chekanov *et al.*, Phys. Lett. **B 549**, 32 (2002).
[8] R. Rückl, Phys. Lett. **B 129** (1983) 363; Nucl. Phys. **B 234** (1984) 91;
W. Buchmuller, R. Rückl and D. Wyler, Phys. Lett. **B 191** (1987) 442;
P. Haberl, F. Schrempp and H. U. Martyn, in *Physics at HERA*, eds. W. Buchmuller and G. Ingelman, DESY (1991) P.1133;
W. Buchmuller and D. Wyler, Phys. Lett. **B 407** (1997) 147 [hep-ph/970431];
N.G.Deshpande, B. Dutta and X.-G. He, Phys. Lett. **B 408** (1997) 288 [hep-ph/9705236].
[9] D. Choudhury, S. Majhi and V. Ravindran, JHEP **0601**, 027 (2006) [hep-ph/0509057];
S. Majhi, arXiv:0705.3071 [hep-ph].
[10] T.G. Rizzo, Phys. Rev. **D 51**, 1064 (1995).
[11] DØ Collaboration, I.A. Bertram, Report No. Fermilab-Conf-96/389-E, (1996).
[12] CDF Collaboration, F.Abe *et al.*, Phys. Rev. Lett. **72**, 3004(1994).
[13] CDF Collaboration, F.Abe *et al.*, Phys. Rev. **D 74**, 3538(1995).
[14] T. Affolder *et el.*, Phy. Rev. Lett. **87**, 231803(2001).
[15] B. Abbott *et el.*, Phy. Rev. **D 62**, 031101(2000).
[16] S. Ferrag on behalf of ATLAS and CMS Collaboration,"*Search for Compositeness at LHC*", Journal of Physics: Confernece Series **110**(2008)072010.
[17] Ben Lillie, Jing Shu and Tim M.P. Tait,"*Top compositeness at the Tevatron and LHC*", **JHEP 04**(2008) 087.
[18] V.M. Abazov *et al.*, "*Measurement of the Isolated Photons Cross Section in p-pbar Collisons at* $\sqrt{s}$ = 1.96 *TeV*", Phys. Lett. **B 639** (2006) 151-158.
[19] B. Abbott *et al.*, "*Comparision of the isolated direct photon cross sections in p-pbar collisions at* $\sqrt{s}$ *=1.8 TeV and* $\sqrt{s}$ *=0.63 TeV*", Phys. Rev. Lett. **84**(2000) 2786-2791.
[20] D. Acosta *et al.*, "*Direct Photon Cross-section with conversions at CDF*", Phys. Rev. **D 70** (2004) 074008.
[21] L. Apanasevich *et al.*, "*Evidence for Parton* K_T *Effects in High-* P_T *Particle Production*", Phys. Rev. Lett. **99** (2007)1217801.
[22] N. Arkani-Hamed *et al.*, "*The Hierarchy Problem and the New Dimensions at a Millimeter*", Phys. Lett. **B 429** (1998) 263-272.
[23] J. Weng *et al.*, "*Search for ADD direct graviton emission in photon plus missing transverse energy final state at CMS*", CMS **Note-2006/129**.
[24] DØ Collaboration, B. Abbott *et al.*, "*Search for large extra dimensions in dielectron and diphoton production*", Phys. Rev. Lett. **86**, 1156 (2001) [arXiv:hep-ex/0008065];
CDF Collaboration, A. A. Affolder *et al.*,"*Search for narrow diphoton resonances and for* $\gamma\gamma + W/Z$ *signatures in* $p\bar{p}$ *collisions at* $\sqrt{s} = 1.8$ *TeV*", Phys. Rev. **D 64**, 092002 (2001) [arXiv:hep-ex/0105066];
[25] P. Hasenfratz and J. Nager, Z. Phys. **C 37**, 477 (1988).
[26] T. Sjostrand *et al.*, Comput. Phys. Commun. 135 (2001)238.
[27] CTEQ Collaboration, H. L. Lai *et al.*, Eur. Phys. J. **C 12**, 375 (2000). [arXiv:hep-ph/9903282].
[28] CMS Collaboration, "*CMS Physics Technical Design Report Vol-I*", CERN/LHCC 2006-001 (2006).
[29] M. Pieri *et al.*, CMS **Note-2006/112**.
[30] CMS Collaboration, "*CMS ECAL Technical Design Report*", CERN/LHCC 97-33.
[31] S. Bhattacharya, S.S. Chauhan, B.C. Choudhary and D. Choudhury, Phys. Rev. **D 76** (2007) 115017.
[32] G. C. Blazey *et al.*, "Run II Physics", hep-ex/0005012 v2 (2000).
[33] CMS TriDAS Project Data Acquisition and High-Level Trigger Technical Design Report CERN/LHCC 2002-26 CMS TDR 6.2.
[34] S. V. Chenkov, "*Jet algorithms: A mini review*", hep-ph/0211298.
[35] S. Catani, Y.L. Dokshitzer, M. H. Seymour, B. R. Webber, Nucl. Phys. **B 406** (1993) 187.
[36] J.M. Butterworth, J. P. Couchman, B. E. Cox and B. M. Waugh, Comput. Phys. Commun. **153** (2003) 35 [hep-ph/0210022].
[37] S.D. Ellis and D.E. Soper, Phys. Rev. **D 48**(1993) 3160 [hep-ph/9305266].
[38] G. Arnison *et al.*, Phys. Lett. **132** (1983) 214.
[39] P. Schieferdcker *et al.*, "*Performance of Jet Algorithms in CMS*", CMS **Analysis Note-2008/001**.
[40] CMS Collaboration, "*CMS HCAL Technical Design Report*", CERN/LHCC 97-31.
[41] ATLAS Collaboration, "*Detector and Physics Performance Technical Design Report*", CERN/LHCC 99-14.
[42] K. O. Mikaelian, M. A. Samuel and D. Sahdev, Phys. Rev. Lett. **43**, 746 (1979).
[43] M.A. Samuel and T. Abraha, [arXiv:hep-ph/970633v1];

U. Baur, S. Errede and G. Landsberg, Phys. Rev. **D 50** (1994) 1917;
V.M. Abazov *et al.*, "*First Study of the radiaton-amplitude zero in $W\gamma$ production and limit on $WW\gamma$ couplings at $\sqrt{s}$ =1.96 TeV*" [arXiv:hep-ex/0803.0030v2]

[44] P. Gupta *et al.*, Eur. Phys. J. C **53**, 49-58(2008).

[45] L. Fano (On behalf of CMS collaboration), CMS **Conference Report -2006/083**.

[46] Jerzy Neyman, Egon Pearson,"*On the Problem of the Most Efficient Tests of Statistical Hypotheses*"- Philosophical Transactions of the Royal Society of London - Series A - Vol 231 (1933) pp. 289-337.

[47] ALEPH Collaboration, DELPHI Collaboration, L3 Collaboration, OPAL Collaboration and The LEP Working Group for Higgs Boson Searches, Phys. Lett. **B 565**(2003) 61.

[48] Maurice G. Kendall, Alan Stuart, The Advanced Theory of Statistics, Vol. 2, "*Inference and Relationships*", Hafner Publishing Company, New York, 1961.

[49] A. L. Read, "*Presentation of Search Results: The CL_s Technique*", J. Phys.G: Nucl. Part. Phys. **28**, 2693-2704 (2002).

[50] F. James, MINUIT - Function Minimization and Error Analysis, CERN Program Library Long Writeup **D506**, 1998.

[51] *http : //root.cern.ch/drupal/content/users − guide*

[52] J. Pumplin, D. R. Stump, J. Huston, H. L. Lai, P. Nadolsky and W. K. Tung, JHEP **0207** (2002) 012 [arXiv:hep-ph/0201195].

[53] A.D. Martin, R.G. Roberts, W.J. Stirling and R.S. Thorne, Eur. Phys. J. C**23**(2002) 73.

[54] P. Bartialini, R. Cheirici and A. De Roeck, "*Guidelines for the Estimation of Theoretical Uncertainties at the LHC*", CMS **Note -2005/115** (2005).

[55] PHOX programs. http://lapweb.in2p3.fr/lapth/phox+family/main.html.

[56] P. Aurenche, M. Fntannaz, J. P. Guillet, E. Pilon, and M. Werlen, Phys. Rev. **D 73**, 094007(2006).

[57] DØ Collaboration, V. M. Abazov *et al.*, arXive:0804.1107v2[hep-ex] 2008.

[58] S. Catani, M. Fontannaz, J. P. Guillet and E. Pilon, JHEP**05** (2002) 0820.

[59] Z. Bern, L. Dixon, C. Schmidt, Phys. Rev. **D 66**, 074018 (2002).

[60] CMS Collaboration, "*CMS Physics Technical Design Report Vol-II*", Jour. of Phys. G **34** (2007) 995-1580.

[61] S. Abdulin *et al.*, CMS **Note-2006/122**.